Xe nuclear magnetic resonance line shapes in nanochannels

Cynthia J. Jameson
Department of Chemistry M/C-111, University of Illinois at Chicago, Chicago, Illinois 60607-7061

Angel C. de Dios
Department of Chemistry, Georgetown University, Washington, DC 20057-2222

(Received 9 July 2001; accepted 4 December 2001)

The intermolecular nuclear magnetic resonance (NMR) chemical shifts of Xe in nanochannels of various dimensions and shapes are considered. Predictions of the line shapes that result from anisotropic averaging of the shielding tensor for Xe atoms in various limiting cases of nanochannels are made, based on *ab initio* calculations of ^{129}Xe shielding surfaces. Variation of the line shapes with channel cross sections, Xe loading, and with temperature are predicted for channels having cross-sectional areas that do not permit two or more Xe centers to be located on the same cross-sectional plane. It is shown that Xe in effectively one-dimensional channels should be expected to exhibit signature line shapes in ^{129}Xe NMR spectra, provided that the cross-sectional dimensions of the channels are sufficiently small that Xe atoms do not pass each other during diffusion. These predictions are tested against experimental examples of anisotropic Xe line shapes in various cavities and nanotubes. © *2002 American Institute of Physics.*
[DOI: 10.1063/1.1446424]

I. INTRODUCTION

The nuclear magnetic resonance (NMR) chemical shift of a Xe nucleus is a widely used probe of intermolecular interactions, structure of materials, distributions of sorbate molecules, and other phenomena. For a Xe atom, intermolecular interactions directly affect the electronic environment of the observed NMR nucleus, leading to two important advantages.

(1) The intermolecular chemical shifts are larger and more exquisitely discriminating between electronic environments.
(2) The theoretical interpretation is more straightforward than that for a molecular probe.

The intrinsically wide range of Xe chemical shifts permits discrimination between electronic environments in gases, in solution, in crystalline or amorphous solids, and in heterogeneous mixtures. The size of the Xe atom is appropriate for entry into nanochannels and cavities. In confined spaces, the distribution of chemical shifts also provide information about sizes and shapes of cavities, numbers of other sorbate molecules within the same cavity as the Xe atom, and distributions of Xe between heterogeneous phases.

Since the chemical shift is a tensor property, the distribution of chemical shift tensor components along the laboratory z axis (magnetic field direction) provides additional information about the nature of the confined geometry. In order to take advantage of this type of information, it is necessary to develop the theoretical connection between the observed Xe chemical shift distributions and the size and shape of the nanochannels and cavities. This is the purpose of this paper.

Some of the models that have been used for interpretation of ^{129}Xe chemical shifts (where σ_0 is the shielding of the isolated Xe atom) are the following:

(1) The Raynes, Buckingham, and Bernstein model[1] (see Ref. 2 for discussion) included a sum of contributions from bulk susceptibility, electrical effects, magnetic anisotropy, and van der Waals interactions

$$\sigma=\sigma_0+\sigma_{\text{bulk susc}}+\sigma_{\text{electric}}+\sigma_{\text{magn aniso}}+\sigma_{\text{vdW}}.$$

In pure Xe gas, after the bulk susceptibility term has been corrected for, there is only the so-called van der Waals contribution. $\sigma_{\text{vdW}}=B\langle F^2(r)\rangle$, where the mean-square fluctuating electric fields associated with dispersion forces are given by an inverse sixth-power dependence on the intermolecular distance, the electric dipole polarizability, and the ionization energy of the bth collision partner

$$\langle F^2(r)\rangle=(3/2)\alpha_b(0)r^{-6}U_X U_b/(U_X+U_b).$$

The parameter B is taken to be the same as that appropriate to the quadratic response of the nuclear shielding to static electric fields, i.e., B is the second derivative of the shielding with respect to the external static electric field.[3]

(2) The reaction field model includes the electric polarization effects from the medium by invoking an Onsager cavity in a uniform continuous medium with dielectric constant $\in$

$$\sigma=\sigma_0+B[f(\in)]^2.$$

First introduced by Buckingham for intermolecular shielding in liquids,[4] it has undergone many adaptations. Rummens[5] introduced the form

$$f(\in)=[(n^2-1)/(2n^2+1)],$$

which has been applied to chemical shifts of Xe in organic solvents.[6]

(3) In zeolites and other nanoporous materials, Fraissard[7] used the model

$$\sigma=\sigma_0+\sigma_{\text{surface}}+\sigma_{\text{Electric}}+\sigma_{\text{Xe–Xe}},$$

where σ_{surface} corresponds to the shielding for Xe at the zero-loading limit, and $\sigma_{\text{Xe–Xe}}$ is assumed to be similar to that in the pure gas and proportional to the number of Xe atoms per cavity. Electrical contributions to shielding are attributed to interactions of Xe with charge-balancing cations in the zeolite.

(4) Also used in zeolites are variations of two-site models such as those that have been proposed by Chen and Fraissard,[8] Cheung,[9] Raftery *et al.*,[10] and S. B. Liu *et al.*[11] In these two-site models, a shielding associated with Xe adsorbed on the surface (σ_{ads}) and a shielding associated with Xe in the free space ($\langle\sigma_{\text{vol}}\rangle$ or σ_{gas}) are averaged over to give the σ_{surface} of the Fraissard model, using mean residence times τ_{surf} and τ_{vol} in the two sites or else fractions of Xe directly adsorbed or otherwise. In Chen and Fraissard's model, the value of the shielding associated with Xe in the free space ($\langle\sigma_{\text{vol}}\rangle$) is itself an average between two successive collisions with the surface and is smaller when the travel distance of xenon is longer. In other words, Xe is assumed to behave as a gas with a definable ''mean free path.'' In the two-site model of Raftery *et al.*

$$\sigma=\sigma_0+[\sigma_{\text{ads}}-\sigma_0]\cdot\tau_{\text{surf}}/(\tau_{\text{surf}}+\tau_{\text{vol}})+[\sigma_{\text{gas}}-\sigma_0]\cdot\tau_{\text{vol}}/(\tau_{\text{surf}}+\tau_{\text{vol}}),$$

τ_{surf}, the residence time on the surface, or the sticking time of Xe on the surface, has a temperature dependence of the form $\tau_{\text{surf}}=\tau_0 e^{[\varepsilon/k\,T]}_B$. On the other hand, the two-site model of Cheung *et al.*[9] is based on the occupancy of the cavity. With N atoms per cavity, N_{sites} adsorption sites per cavity, and fraction θ of adsorption sites being occupied

$$\sigma=\sigma_0+[\sigma_{\text{ads}}-\sigma_0]\cdot(N_{\text{sites}}\theta/N)+[\sigma_{\text{gas}}-\sigma_0]\cdot\{1-(N_{\text{sites}}\theta/N)\},$$

where σ_{gas} is the same as in pure xenon gas and θ is a function of temperature. The two-site exchange model proposed by Liu *et al.* considered the fraction not directly adsorbed as a series expansion in the surface coverage.[11] These various site exchange models are compared with one another in a recent review by Bonardet *et al.*[12]

Some specific objections to these models are as follows: It has been demonstrated that the electric field effects on σ of rare gas atoms are actually rather small. For Xe, the second derivative of shielding with respect to the external electric field, B, has been calculated *ab initio* by Bishop[13,14] and is found to be orders of magnitude smaller than the parameter B in the Raynes, Buckingham, and Bernstein model. Dispersion contributions to shielding can be obtained from the difference between the shielding calculated by a method that explicitly includes electron correlation and that calculated at the Hartree–Fock level. Except when the electronic ground state is degenerate, the dispersion contributions are not expected to dominate intermolecular shifts. The highest level of shielding calculation for Ne–Ne (at the coupled-cluster singles and doubles with some triple excitations) gives results that are very close to Hartree–Fock level shielding calculations.[15] Intermolecular chemical shifts of Xe cannot be largely attributed to dispersion contributions since *ab initio* calculations of Xe shielding surfaces at a level that does not explicitly include dispersion contributions (Hartree–Fock level) give results that account for most of the observed density coefficients of the gas phase Xe chemical shifts. The second model, the reaction field model, attributes all intermolecular shifts to electric polarization effects. These are likewise insufficiently large to account for most of intermolecular shielding. Reaction field models, even the ones including higher multipoles, are unable to reproduce the orders of magnitude of many gas-to-liquid shifts where specific interactions between molecules play a role.[16–19] The model for Xe chemical shifts proposed by Fraissard enumerates contributions but does not permit calculations of Xe chemical shifts. By separately calculating shielding contributions from Xe–zeolite interactions and Xe–Xe interaction, we have shown[20,21] that the former (literally σ_{surf}) are not independent of n_{Xe} and $\sigma_{\text{Xe–Xe}}$ is not directly proportional to n_{Xe}, as has been assumed in the Fraissard model. The fourth class of models, two-site models, are physically incorrect, since Xe is found in a very large number of configurations inside of a cavity, not just at the lowest energy adsorption site, or in the center of the cavity, or the free gas. To find the average shielding, one needs to do a weighted average over all configurations, not just ''at the adsorption site'' versus off-site. At best these models are inadequate for quantitative interpretation, although they may appear to follow some experimental trends. Where possible, in our past work, we interpreted experimental data using simulations and calculations as close as possible to first principles. In doing so, we have established the isotropic Xe shielding in various zeolites, as a function of temperature and composition in binary adsorption mixtures as more severe tests of molecular simulations in nanoporous materials than adsorption isotherms or isosteric heats alone.[20–28] Furthermore, we would like to predict new experimental observations, and these models do not afford such predictions.

In some confined spaces, an anisotropic line shape in the NMR spectrum of the Xe atom has been observed, in clathrates, and in one-dimensional channels.[25,29–37] Models that have been proposed to account for the line shapes in ^{129}Xe NMR spectra of Xe in nanotubes include the following:

(1) The channel or cavity molds the Xe electron cloud. The shape of the electron cloud is the shape of the shielding tensor itself (prolate, oblate, spherical).[34]

(2) Xe interactions with charge compensating cations polarizes the Xe cloud and reduces the symmetry of the Xe atom.[34]

(3) A Xe atom adsorbed to a channel surface has a locally axial shielding tensor, and the intensity profile resulting from the distribution of adsorption sites in a cylindrical channel is a consequence of the relative surface areas of the cylinder versus the end caps.[31]
(4) An average over a binomial distribution of Xe into adsorption sites, each site with a characteristic shielding tensor according to whether neighboring sites are occupied or not, results in the average line shape.[32]

Model 1 is clearly incorrect; it is based on the wrong notion that the shielding tensor and electron density are directly related. While SAPO-11 and ALPO-11 differ in that SAPO-11 has charge balancing cations, the line shapes of Xe are very similar in these two molecular sieves which have the same channel shape and size. Thus, polarization by cations cannot be the factor that determines the Xe line shape. We shall see from *ab initio* calculations in model systems that Xe adsorbed to a surface does not necessarily have an axial shielding tensor. Furthermore, Xe is not immobilized on the surfaces. Ripmeester and Ratcliffe's model 4 seems the only viable one of these interpretations, although it too is based on classifying Xe atoms as either in an adsorption site or not.

In this paper, we propose to predict the NMR line shapes of Xe in nanochannels. Our approach is as follows: (a) We use *ab initio* calculations of intermolecular shielding tensors of Xe as the basis for predicting the changes in the tensor components with distance and site symmetry; (b) we consider Xe line shapes in limiting cases where symmetry dictates the principal axis directions of Xe shielding tensors in nanochannels; (c) we use correlation diagrams to follow the systematic progression of the shielding tensor components from one limiting case to another; (d) we make predictions for line shapes of Xe in a variety of open indefinitely long nanochannels, in capped nanopipes, and in disks, as a function of loading and as a function of temperature; and (e) finally, we compare predictions with realistic experimental cases.

II. THE NATURE OF THE Xe INTERMOLECULAR SHIELDING TENSOR SURFACE FROM *AB INITIO* CALCULATIONS

The general shape of the mathematical surface that describes the intermolecular shielding tensor as a function of molecular configuration has been discussed in Ref. 2. The general trends are obtained by calculations on Ar shielding in Ar–Ar for a very wide range of distances, e.g., the isotropic intermolecular shielding is sketched in Fig. 1. The same shapes have been obtained for all pairs of rare gas atoms.[38] Calculations for rare gas atom and linear molecules reveal the same general behavior of the individual tensor components as for rare gas pairs.[39]

Shielding calculations were performed in the GIAO scheme at the Hartree–Fock level, using a parallel version of the GAUSSIAN 98 program.[40] Xenon was provided an uncontracted $29s21p17d9f$ basis set. The core ($26s19p13d$) was taken from Partridge and Faegri[41] and these were augmented by additional $3s$, $2p$, $4d$, $9f$ orbitals with exponents taken from Bishop,[42] who had used these functions in shielding

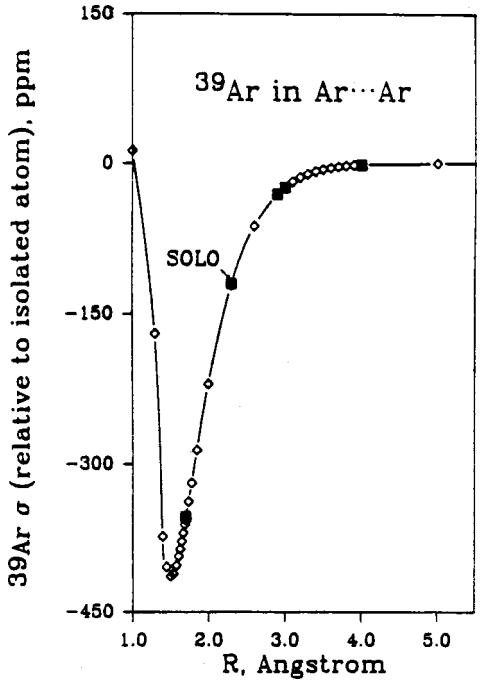

FIG. 1. The general shape of the intermolecular shielding tensor for Ar in the presence of another Ar atom, from our previous calculations, reproduced from Ref. 2.

calculations of Xe atom in the presence of a uniform electric field. This basis set of 240 basis functions on Xe is sufficiently large so that the counterpoise corrections to the Xe shielding are negligible [of the order of $+0.03$ ppm where the intermolecular shielding is -63.35 ppm (0.05%) and $+0.0006$ ppm where the intermolecular shielding is -5.0804 ppm (0.01%)]. The same basis set had been used by us for the calculations of Xe shielding for the Xe(CO_2), Xe(N_2), Xe(CO), and other systems previously published, selectively used here as examples to develop the general insights into Xe line shapes in nanochannels. These calculations used $11s7p3d$ contracted to $7s/6p/3d$ for C and O atoms, $11s$, $7p$ Huzinaga basis in the contraction $(5,6\times1;2,5\times1)$ augmented by three sets of d functions.[43] For the Xe in a ring calculations, neon was assigned a standard 6-311 G basis set with two sets of d-type polarization functions and one set of diffuse functions. These computations were carried out on an Origin 2000 machine (Silicon Graphics, Inc.) equipped with four processors. A single-point shielding calculation on the xenon trimer (all tensors for one chosen configuration of the trimer), the largest calculations reported in this paper was, completed in 3 days on this computer on average.

We illustrate the general behavior of the individual Xe shielding tensor components upon interaction of the Xe with an atom, a molecule, a line of atoms, and a ring of atoms. We begin with the results of *ab initio* calculations of ^{129}Xe shielding surfaces for Xe–Xe, shown in Table I. These results reveal the following general behavior: As the intermolecular partner gets closer, the component of the shielding tensor along its direction of approach changes little, increasing shielding slightly. On the other hand, uniformly, the tensor components in the plane perpendicular to the direction of approach become less shielded. This is the same behavior

TABLE I. *Ab initio* shielding of ^{129}Xe in Xe–Xe system as a function of distance, in ppm relative to the free Xe atom.

R(Xe–Xe), Å	$\sigma_\parallel-\sigma$ (Xe atom)	$\sigma_\perp-\sigma$ (Xe atom)	$\sigma_{iso}-\sigma$ (Xe atom)	$\sigma_\parallel-\sigma_\perp$
3.0	+6.14	−742.87	−493.20	749.01
3.2	+5.06	−518.02	−343.66	523.08
3.4	+4.22	−353.80	−234.46	358.02
3.6	+3.55	−237.10	−156.88	240.65
3.8	+3.02	−156.13	−103.08	159.15
4.0	+2.53	−101.19	−66.60	103.77
4.4	+1.94	−40.79	−26.55	42.73
4.8	+1.49	−15.77	−10.02	17.27
5.2	+1.17	−5.98	−3.60	7.16
6.0	+0.76	−0.97	−0.39	1.73
7.0	+0.48	−0.24	−0.003	0.72
∞	0.0	0.0	0.0	0.0

obtained for ^{129}Xe shielding tensors in the pairs Xe–Xe, Xe–Kr, Xe–Ar, and Xe–Ne,[44] as well as for Ar–Ar[2] and Ar–Ne.[45] Indeed, the same behavior has also been found when considering the response of the Xe shielding to the colinear approach of a linear molecule,[39] as shown by a small selection of the *ab initio* results in Table II for Xe approaching the OCO, CO, and NN molecules end on, with the order being $\sigma_\perp<\sigma_\parallel\approx\sigma$ (free Xe atom) at all distances. *In all cases, the components of the shielding tensor in the plane perpendicular to the direction of approach are uniformly deshielded, whereas the tensor component along the direction of approach is changed only slightly*.

We also examine a very simple model for how the shielding tensor of a Xe atom is changed by the presence of a wall of atoms. We use here the *ab initio* results for the Xe shielding response to the approach of a CO_2 molecule in a T formation. In Table III we present the full shielding tensor for the Xe–CO_2 system in a T configuration at four distances. Imagine that the CO_2 is a line of atoms that constitutes a nanochannel, and the Xe atom is at a distance R(Xe–C) from the channel wall. For this specific example, the three shielding tensor components are labeled as follows: The parallel component ($\sigma_\parallel$) is along the direction parallel to the OCO molecule axis. The perpendicular component ($\sigma_\perp$) is perpendicular to the wall (i.e., along the Xe–C line) and the component tangential to the wall (σ_t) is perpendicular to the molecular plane of the supermolecule. The *ab initio* results show that *all components are deshielded relative to the Xe atom* with the order being $\sigma_\parallel<\sigma_t<\sigma_\perp$. *The least deshielding occurs for the component along the line of approach of the Xe to the wall*, and this component is deshielded relative to the free Xe atom at distances close to the equilibrium configuration of the van der Waals molecule, becoming only slightly more shielded than the free Xe at longer distances. Suppose the wall is constituted of the same atoms (C and O) but with a different electronic structure. Does the Xe shielding tensor distinguish between the two walls? To answer this question, we present the *ab initio* Xe shielding tensor in the Xe(CO) configuration where the vector from the Xe to the center of mass of the CO molecule is 90° relative to the CO molecular axis. Using the same definitions for the tensor components as in the Xe–CO_2 system, we present the data in Table IV. We find that the intermolecular shielding tensor components are in the same order as in the Xe–CO_2 system, $\sigma_\parallel<\sigma_t<\sigma_\perp$ at all distances, but the $\sigma_\parallel$ and σ_t deshielding effects are more pronounced for Xe(CO) than for Xe–CO_2 at the same distances. The Xe shielding tensor components can distinguish easily between walls of different electronic structure, even when the constituent atoms are the same.

Another contrast is provided by Xe approaching O atoms that are bridging atoms in an aluminosilicate fragment. The bonding of the O atoms in bridging positions is substantially different from either CO or CO_2. The results of *ab initio* calculations are shown in Table V. There are many more atoms making up the nanochannel ''wall'' in this example. At

TABLE II. *Ab initio* shielding of ^{129}Xe in collinear Xe–linear molecule systems, ppm relative to the free Xe atom. The parallel component ($\sigma_\parallel$) is along the direction of approach and $\sigma_\perp$ are in the plane perpendicular to the direction of approach (Ref. 39).

System	R(Xe–A), Å	$\sigma\parallel-\sigma$ (Xe atom)	$\sigma\perp-\sigma$ (Xe atom)	σiso$-\sigma$ (Xe atom)	$\sigma_\parallel-\sigma_\perp$
Xe···OCO	3.0	+1.8315	−85.8696	−56.6359	87.7011
Xe···OCO	3.4	+1.2798	−33.3644	−21.8163	34.6442
Xe···NN	2.85	+1.9715	−270.1380	−179.4348	272.1095
Xe···NN	3.25	+1.3287	−111.0405	−73.5841	112.3694
Xe···OC	3.0	+1.6402	−95.8201	−63.3336	97.4603
Xe···OC	3.4	+1.1277	−37.5445	−24.6538	38.6722
Xe···CO	3.0	+1.7246	−380.1533	−252.8607	381.8779
Xe···CO	3.4	+1.1937	−159.9324	−106.2237	161.1261

TABLE III. *Ab initio* shielding tensor components of ^{129}Xe in Xe–CO_2 system in the *T*-shaped configuration, *a model for Xe atom on a wall*, in ppm relative to the free Xe atom. The component $\sigma_\parallel$ is along the direction parallel to the wall, (i.e., parallel to the OCO molecule axis), the $\sigma_\perp$ is perpendicular to the wall (i.e., along the Xe–C line), and the component tangential to the wall (σ_t) is perpendicular to the molecular plane of the supermolecule (Ref. 39).

R(Xe–C), Å	$\sigma_\parallel-\sigma$ (Xe atom)	$\sigma_t-\sigma$ (Xe atom)	$\sigma_\perp-\sigma$ (Xe atom)	$\sigma_{iso}-\sigma$ (Xe atom)
3.0	−113.1499	−94.4160	−20.7109	−76.0923
3.4	−48.3364	−24.3032	−7.119	−26.5862
4.0	−11.6448	−1.9021	−0.7836	−4.7768
4.8	−1.5811	−0.0221	+0.3782	−0.4083

TABLE IV. *Ab initio* shielding tensor components of ^{129}Xe in Xe(CO) system in the T-shaped configuration, *a model for Xe atom on a wall*, in ppm relative to the free Xe atom. The component $\sigma_\parallel$ is along the direction parallel to the CO molecular axis), the $\sigma_\perp$ is perpendicular to the wall (i.e., along the line joining the Xe to the center of mass of the CO molecule), and the component tangential to the wall (σ_t) is perpendicular to the molecular plane of the supermolecule (Ref. 39). R(Xe–cm) is the distance between Xe and the center of mass of the CO molecule.

R(Xe–cm), Å	$\sigma_\parallel-\sigma$ (Xe atom)	$\sigma_t-\sigma$ (Xe atom)	$\sigma_\perp-\sigma$ (Xe atom)	$\sigma_{iso}-\sigma$ (Xe atom)
3.0	−414.8754	−206.1174	−5.2387	−208.7438
3.4	−167.4693	−90.8485	−1.2296	−86.5158
4.0	−38.3636	−22.9075	+0.1393	−20.3773
4.8	−4.5645	−3.0623	+0.2454	−2.4605

TABLE V. Xe shielding tensor components for four configurations of Xe atop an O atom, in ppm relative to the free Xe atom.

R(Xe–O), Å	$\sigma_{t'}-\sigma$ (Xe atom)	$\sigma_t-\sigma$ (Xe atom)	$\sigma_\perp-\sigma$ (Xe atom)	$\sigma_{iso}-\sigma$ (Xe atom)
XE above O atom in an 8-ring of zeolite cage:				
3.21	−348.6	−259.8	−159.0	−255.8
4.28	−62.2	−47.5	−8.9	−39.5
Xe above O atom in a 6-ring of zeolite cage				
3.21, O_1	−174.5	−141.7	−56.8	−124.3
3.21, O_2	−189.6	−175.0	−68.8	−144.5

the same time, the wall is not at all flat but very corrugated, since the bridging O atoms have Si–O–Al bond angles that are very different from 180°. For illustration, we select four configurations with Xe sitting atop three types of O atom sites in these aluminosilicate fragments. There are two components that may be denoted tangential to the aluminosilicate wall ($\sigma_{t'}$ and σ_t) and the third one is perpendicular to the wall ($\sigma_\perp$). Here again, we find that *the component along the direction of approach is the least deshielded component*, whereas the two tangential components are very deshielded

$$\sigma_{t'}, \sigma_t < \sigma_\perp < \sigma(\text{free Xe atom}).$$

The nanochannels we are considering here can have cross-sectional diameters that are comparable to the size of a small molecule. To model the combined effect on Xe shielding of the interaction of the Xe atom with a ring of atoms constituting the cross section of the channel, we use the simple system of a Xe atom surrounded by 6 Ne atoms which form a regular hexagon. In this model system, $\sigma_\parallel$ is the component perpendicular to the plane of the ring (parallel to the channel), $\sigma_\perp$ is the component along the short Xe–Ne distance (i.e., perpendicular to the wall and the channel axis), and σ_t is the component in the plane of the ring and perpendicular to the short Xe–Ne distance (i.e., tangential to the wall and perpendicular to the channel axis). For the larger ring, the Xe may be located at the center or off-center. We consider the effect of the ring size, and we compare the shielding components for Xe at the same closest Xe–Ne distance (3.0 Å): in the center of the smaller ring versus off-center in the larger ring. The *ab initio* results for the Xe shielding tensor are shown in Table VI.

The important results are as follows: for a Xe atom in the center of the ring

$$\sigma_\parallel < \sigma_\perp < \sigma(\text{free Xe atom}),$$

where $\sigma_\parallel$ is along the axis of the cylinder of which the ring is the cross section. We find that *the* Xe *atom is more strongly deshielded when located in the center of the smaller ring than in the center of the larger ring*. For the same closest Xe–wall distance, the deshielding is greater for the smaller ring than for the larger ring. Here, we find that the larger ring with the same number of atoms does not provide a fair comparison with respect to ring size, since the Ne–Ne distances along the perimeter of the ring are substantially different. A more appropriate comparison is afforded by the ring (4 Å radius) of 8 Ne atoms compared against the ring (3 Å radius) of 6 Ne atoms. We still find that, *for the same closest* Xe–*wall distance, the deshielding is greater for the smaller ring than for the larger ring*. How sharply this deshielding effect drops off with increasing ring size is indicated by the general shape of the intermolecular shielding function for a pair of rare gas atoms. A consequence of this general shape of the intermolecular shielding function, too is that *for the same closest* Xe*-to-wall distance, the deshielding is greater for the smaller ring than for the larger ring.* There are shorter Xe-to-ring atom distances in the smaller ring compared to Xe-to-ring atom distances in the larger ring. Also, we note that the deshielding effect is nearly additive: At the center of the 4 Å ring, Xe experiences a deshielding that is nearly a factor of 8/6 in the center of the Ne_8 ring compared to at the center of the Ne_6 ring.

TABLE VI. *Ab initio* results for the shielding tensor of a Xe atom at the center of a ring of Ne atoms, in ppm relative to the free Xe atom. R_{Xe} is the distance of the Xe atom from the center of the ring. $\sigma_\parallel$ is the component perpendicular to the plane of the ring, $\sigma_\perp$ is the component along the short Xe–Ne distance, and σ_t is the component in the plane of the ring and perpendicular to the short Xe–Ne distance. Also shown are the tensor components that result from summing over individual Xe–Ne shielding tensors.

Model	r_{ring} Å	R_{Xe} Å	$\sigma_\parallel-\sigma$ (Xe atom)	$\sigma_\perp-\sigma$ (Xe atom)	$\sigma_t-\sigma$ (Xe atom)	$\sigma_{iso}-\sigma$ (Xe atom)
$Xe@Ne_6$	3.0	0.0	−136.21	−85.27		−71.02
$\Sigma_i^6 XeNe_i$	3.0	0.0	−171.61	−82.88		−112.45
$Xe@Ne_6$	4.0	0.0	−12.91	−5.69		−8.10
$\Sigma_i^6 XeNe_i$	4.0	0.0	−13.59	−5.64		−8.29
$Xe@Ne_8$	4.0	0.0	−16.00	−7.68		−10.45
$\Sigma_i^8 XeNe_i$	4.0	0.0	−18.12	−7.52		−11.05
$Xe@Ne_6$	4.0	1.0	−40.04	−11.13	−28.86	−26.68
$\Sigma_i^6 XeNe_i$	4.0	1.0	−43.18	−11.45	−29.00	−27.85
$Xe@Ne_8$	4.0	1.0	−47.67	−18.39	−35.48	−33.85
$\Sigma_i^8 XeNe_i$	4.0	1.0	−57.20	−18.69	−34.83	−36.91

Finally, for both the 8-Ne-atom ring and the 6-Ne-atom ring, when the Xe is off-center and 3 Å from the wall, we find that the relative ordering of the components is

$$\sigma_\parallel < \sigma_t < \sigma_\perp < \sigma(\text{free Xe atom}),$$

where $\sigma_\parallel$ is the component perpendicular to the plane of the ring, $\sigma_\perp$ is the component along the short Xe–Ne distance, and σ_t is the component in the plane of the ring and perpendicular to the short Xe–Ne distance.

In summary, the *ab initio* results lead to the following conclusions:

(1) In all cases of Xe interacting with an atom or approaching collinearly to a linear molecule, the components of the Xe shielding tensor in the plane perpendicular to the direction of approach are uniformly deshielded, whereas the tensor component along the direction of approach is changed only slightly.

(2) For Xe interacting with a wall (a line) of atoms, all components are deshielded relative to the Xe atom with the order being $\sigma_\parallel < \sigma_t < \sigma_\perp$ at all distances.

(3) The least deshielding occurs for the component along the line of approach of the Xe to the wall.

(4) For a Xe atom in the center of a ring of atoms, $\sigma_\parallel < \sigma_\perp < \sigma$ (free Xe atom), where $\sigma_\parallel$ is along the axis of the cylinder of which the ring is the cross section.

TABLE VII. ^{129}Xe shielding tensor components calculated for the central atom in Xe_3 systems, in ppm relative to the free Xe atom. $\sigma_\perp$ is the component perpendicular to the line of centers in the linear case and perpendicular to the molecular plane in the triangular case. The two components in the plane of the molecule are along the C_2 axis or perpendicular to the C_2 axis. Estimates for Xe_3 systems from summing over the Xe–Xe contributions given in Table I are compared with the *ab initio* calculations.

r_{Xe-Xe}	4.0 Å			4.4 Å		
Central Xe in Xe_3	$\sigma_\perp$	$\sigma_{(C2)}$	$\sigma_{(\perp \text{ to } C2)}$	$\sigma_\perp$	$\sigma_{(C2)}$	$\sigma_{(\perp \text{ to } C2)}$
$\alpha=180°$	−204.72	−204.72	+5.17	−81.89	−81.89	+3.88
$\alpha=180$, if additive	−202.38	−202.38	+5.06	−81.58	−81.58	+3.88
Dev	−2.3	−2.3	−0.1	+0.3	+0.3	0.0
$\alpha=170°$	−204.79	−203.04	+3.62	−81.91	−81.21	+3.23
$\alpha=170$, if additive	−202.38	−200.80	+3.48	−81.58	−80.93	+3.23
Dev	−2.3	+2.2	−0.1	+0.3	+0.3	0.0
$\alpha=150°$	−205.23	−190.17	−8.52	−82.00	−76.04	−1.84
$\alpha=150$, if additive	−202.38	−188.50	−8.84	−81.58	−75.86	−1.84
Dev	+2.8	+2.0	−0.3	+0.4	+0.2	0.0
$\alpha=120°$	−204.32	−151.04	−46.32	−81.81	−60.29	−17.44
$\alpha=120$, if additive	−202.38	−150.52	−46.80	−81.58	−60.22	−17.48
Dev	+1.9	+0.5	−0.5	+0.2	+0.1	0.0
$\alpha=90°$	−195.17	−98.68	−98.68	−79.89	−38.87	−38.87
$\alpha=90$, if additive	−202.38	−98.66	−98.66	−81.58	−38.85	−38.85
Dev	−7.2	0.0	0.0	−1.7	0.0	0.0
$\alpha=60°$	−159.67	−49.36	−143.94	−70.05	−17.89	−58.51
$\alpha=60°$, if additive	−202.38	−46.80	−150.52	−81.58	−17.48	−60.22
Dev	−42.7	2.6	−6.6	−11.5	0.4	−1.7

(5) The Xe atom is more strongly deshielded when located in the center of a smaller ring than in the center of a larger ring. For the same closest Xe–wall distance, the deshielding is greater for the smaller ring than for the larger ring. This is a consequence of the shorter Xe-to-ring atom distances in the smaller ring.

(6) Finally, for both the 8-Ne-atom ring and the 6-Ne-atom ring, when the Xe is off-center and 3 Å from the wall, we find that the relative ordering of the components is

$$\sigma_\parallel < \sigma_t < \sigma_\perp < \sigma(\text{free Xe atom}),$$

where $\sigma_\parallel$ is the component perpendicular to the plane of the ring, $\sigma_\perp$ is the component along the short Xe–Ne distance, and σ_t is the component in the plane of the ring and perpendicular to the short Xe–Ne distance.

The *ab initio* ^{129}Xe shielding tensor components for a Xe interacting with a single Ne atom has been calculated as a function of distance.[44] Using this shielding function, we can test the additivity of the individual Ne contributions from the ring atoms. Shown in Table VI, immediately below the *ab initio* results for Xe in each ring system, are the results of the summation of tensor components from the components of the Xe–Ne dimer alone, using the angles made by the individual Xe–Ne vectors relative to the principal axis directions of the Xe shielding tensor in the Ne_6 or Ne_8 ring system. For $\sigma_\parallel$, the assumption of additivity leads to errors in the range of 5%–26% at these distances. The largest deviation is in the $\sigma_\parallel$ parallel to the axis of symmetry of the small Ne_6 ring. Nevertheless, the additivity assumption is quite good, leading to correct predictions of relative magnitudes of the principal components in every case.

Finally, we consider *ab initio* calculations of the Xe shielding tensor in the presence of two Xe atoms, as a model for the Xe in a pipe at high loading. In the case where Xe–Xe interactions dominate the shielding tensor, compared to the Xe–wall interactions, the Xe trimer serves as a good model. We show the results for Xe_3 in a linear configuration, in a symmetrical triangular configuration and also as a function of angle in a C_{2v} configuration in Tables VII and VIII. In the case of Xe_3 with $\alpha=60°$, there is no distinction between the terminal and the center Xe; the shielding tensor is the same for all Xe nuclei in this case. In Table VII, it is shown that the shielding tensor components for the central Xe can be estimated remarkably well by adding up the contributions from the Xe–Xe shielding tensor given in Table I, except for the 60° case where all Xe atoms are equidistant and the interactions between the terminal Xe atoms can no longer be neglected. Similarly, the shielding tensors of the terminal Xe in the Xe_3 systems (shown in Table VIII) are well predicted by neglecting contributions from the other terminal Xe atom; the tensor components are all very similar to the values in Table I for the Xe_2 dimer. All principal axes for terminal Xe deviate only slightly from axially symmetric about the Xe–Xe ''bond'' direction. The terminal Xe shielding tensors all have slightly larger span of the shielding by about 0.8 ppm at 4 Å and 0.4 ppm at 4.4 Å, except for the 60° case, where the interactions between the two terminal Xe atoms are identical to the interaction between the central and terminal Xe. We will make use of these results in understanding the Xe shielding in nanochannels under full loading.

These findings are consistent with the deshielding diminishing sharply with distance in the general shape of the intermolecular shielding function for a pair of rare gas atoms. With the quantitative insight gained from the *ab initio* results of shielding tensors for Xe in simple model systems, we now consider predicting the Xe line shape that would be observed in various limiting cases of nanochannels such as indefinitely

TABLE VIII. ^{129}Xe shielding tensor components calculated for the terminal atom in Xe_3 systems, in ppm relative to the free Xe atom. Estimates for Xe_3 systems neglecting contributions from the other terminal atom are compared with the *ab initio* calculations. $\sigma_\perp$ is the component perpendicular to the line of centers in the linear case and perpendicular to the molecular plane in the triangular case. The two components in the plane of the molecule are nearly along r_{Xe-Xe} and the other (σ_{other}) is perpendicular to it.

r_{Xe-Xe}	4.0 Å			4.4 Å		
Terminal Xe Xe_3	$\sigma_\perp$	σ_{other}	$\sigma_\parallel$ $\parallel$ to r_{Xe-Xe}	$\sigma_\perp$	σ_{other}	$\sigma_\parallel$ $\parallel$ to r_{Xe-Xe}
If additive, and neglect the other terminal Xe	−101.19	−101.19	+2.53	−40.79	−40.79	+1.94
$\alpha=180°$	−101.66	−101.66	+2.91	−40.90	−40.90	+2.18
$\alpha=170°$	−101.62	−101.65	+2.91	−40.87	−40.90	+2.18
$\alpha=150°$	−101.50	−101.61	+2.89	−40.87	−40.81	+2.18
$\alpha=120°$	−101.93	−101.52	+2.86	−41.06	−40.90	+2.20
$\alpha=90°$	−101.94	−101.48	+2.25	−41.27	−40.78	+2.01

long pipes with smooth structureless walls, parallel plates, capped pipes, disks, and cavities. Then, in Sec. IV we compare our predictions with observed line shapes for Xe in nanochannels of various types.

III. LIMITING CASES OF LINE SHAPES FOR Xe IN NANOCHANNELS

A. At the zero-loading limit

1. Case A (smooth narrow-bore pipe)

We consider a continuously *smooth* (not atomistic) pipe having radius r such that Xe minimum energy position is along the center of the pipe cross section. The pipe has no corrugation, so there is no change in either potential energy or the shielding tensor with respect to position of Xe along the axis of the pipe. Since this is the case, the isotropic shielding and the line shape *should be temperature independent*. The anisotropy of the shielding tensor results from the interaction of the Xe atom with the smooth wall: the component perpendicular to the wall and parallel to the axis of the pipe ($\sigma_\parallel$, that is, parallel to the axis of the pipe) is less shielded (paramagnetic contribution arising from deformation from spherical symmetry gives this). On the other hand, the components lying in the cross-sectional plane ($\sigma_\perp$) do not have this large paramagnetic contribution since there are no atoms on the axis, either above or below the plane. The component $\sigma_\perp$ is more shielded by a small amount compared to the free Xe atom due to the $\langle[x^2+y^2]/r^3\rangle$ values for a deformed Xe atom differing from that in the free atom. If the electron density becomes football-shaped (prolate), the diamagnetic contributions should be larger for the equatorial component than for the axial component. If the electron density becomes disk-shaped (oblate), the diamagnetic contributions should be larger for the axial component. Thus, the principal tensor components are in the directions shown in Fig. 2; the tensor is expected to be axial with components in the following order relative to the free Xe atom:

$$\sigma_\parallel < \sigma_\perp < \sigma(\text{free Xe atom}).$$

2. Case B (narrow-bore pipe)

If the pipe is not continuously smooth but has atomistic structure, and r_{pipe} is small enough that the Xe minimum energy position is at the center of the pipe, along the axis, varying with z, the tensor σ will be axial at each z, if symmetry at the cross-sectional plane is threefold or higher. The potential energy of a Xe atom U (Xe in pipe) will be a function of z, therefore, in this case the line shape will be the same (axial anisotropy) but the span will change with z. (If the symmetry at the cross-sectional plane is lower than threefold, then it is unlikely that the Xe minimum energy position will remain along the central axis of the pipe for all z.) The temperature dependence arises from the potential energy surface of Xe in the pipe varying with z.

3. Case C (smooth medium-bore pipe)

Our definition of ''medium-bore'' is that the cross section of the pipe does not permit two Xe centers to be located in the same cross-sectional plane. Xe in a continuous *smooth* pipe with a circular cross section will have its minimum energy position along a locus of points that constitutes a cylinder coaxial with the pipe. In this case, the tensor will no longer be axial. As shown in the bottom of Fig. 3, two components are in directions tangential to the wall surface (σ_t and $\sigma_{t'}$) and the third component ($\sigma_\perp$) is perpendicular to the wall surface. One tangential component will be parallel to the pipe axis ($\sigma_\parallel$ is $\sigma_{t'}$) by symmetry; σ_t is seen in Fig. 3

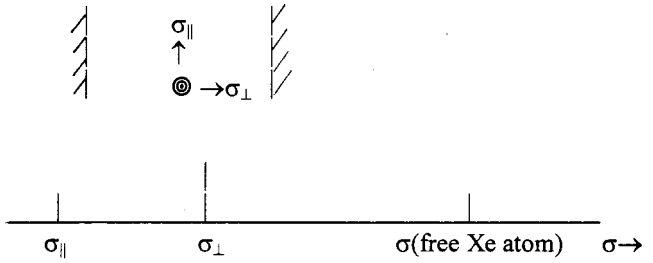

FIG. 2. The expected shielding components for a single Xe in a smooth narrow-bore pipe.

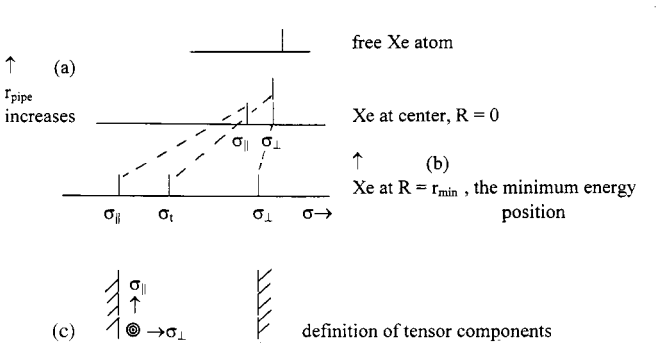

FIG. 3. The correlation diagram of shielding components of a single Xe in a smooth medium-bore pipe (a) for Xe at the center of the pipe ($R=0$) as r_{pipe} increases, and (b) for Xe at position R, as R approaches $r_{\min}$ (the position of minimum energy for Xe in the pipe), and (c) the temperature dependence of the thermal average shielding for Xe in a medium-bore pipe.

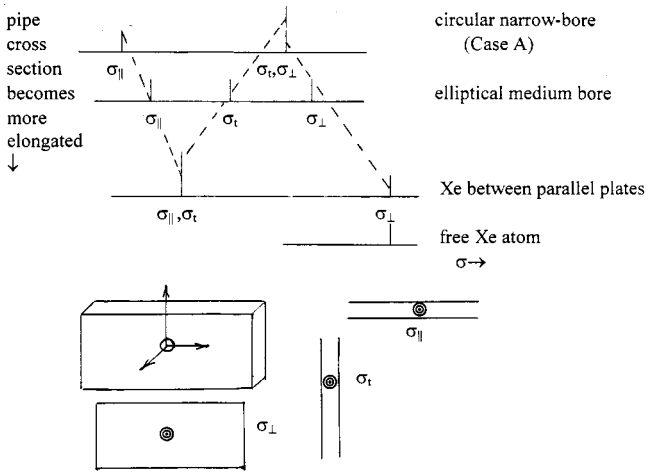

FIG. 4. The correlation diagram of shielding components of a single Xe in a pipe, as the pipe cross section becomes more elongated, from the limiting case of the circular narrow-bore pipe to the limiting case of Xe between parallel uniform plates.

as an arrowhead coming out of the paper. The two tangential shielding components are expected to be less shielded since most of the Xe interactions will be directed perpendicular to the surface of the wall. The $\sigma_\parallel$ component will include interactions with an entire arc of the wall in the cross-sectional plane and will be the most deshielded component. The component $\sigma_\perp$ should not be as greatly deshielded, especially as the Xe moves away from the wall, since there are no other atoms along the pipe axis. Nevertheless, $\sigma_\perp$ will be deshielded compared to free Xe atom since the wall is not planar. Thus, for a single Xe atom located at the minimum energy distance $R=r_{\min}$ from the center of the medium-bore pipe, the tensor components are in the following order relative to the free Xe atom:

$$\sigma_\parallel<\sigma_t<\sigma_\perp<\sigma(\text{free Xe atom}).$$

In the special case of a single Xe atom located in the center of the pipe ($R=0$), the tensor is axial. Figure 3(a) shows the change in the components for a Xe located at the center as the radius of the pipe r_{pipe} gets larger, both components of σ approach that of free Xe atom. Figure 3(b) shows the systematic change in the shielding tensor as the Xe atom moves from its minimum energy position at $R=r_{\min}$ towards the center of the pipe: the tangential component σ_t becomes the same as the component $\sigma_\perp$.

Let us now consider a pipe of elliptical cross section. It is helpful to consider going to the limiting case of an ellipse with very large eccentricity, until the pipe approaches the limit of two parallel plates. For a single Xe atom trapped between two parallel plates, the definition of the tensor components is shown at the bottom of Fig. 4. The most shielded component is $\sigma_\perp$; since there are no interactions with Xe in this plane, $\sigma_\perp$ should be identical to σ (free Xe atom). $\sigma_\parallel$ and σ_t are exactly equivalent for Xe trapped between two parallel plates. The other limiting case, as the ellipse approaches a circle, is that which we have already considered, case A. $\sigma_\parallel$ and σ_t become more similar as the long axis of the ellipse gets longer. In going from the Xe between parallel plates to the pipe of elliptical cross section, $\sigma_\perp$ becomes less shielded than the free Xe atom, and σ_t moves away from $\sigma_\parallel$ toward the other limit (case A, where it ultimately becomes identical with $\sigma_\perp$). Thus, we find for Xe in an elliptical medium-bore pipe

$$\sigma_\parallel<\sigma_t<\sigma_\perp<\sigma(\text{free Xe atom}).$$

We also expect $\sigma_\parallel$ to become systematically more deshielded in going from the parallel plates, to the elliptical-bore pipe, to the narrow-bore pipe. The relative magnitudes of the shielding tensor components of Xe in these cases are shown in Fig. 4.

4. Case D (medium-bore pipe)

As in case C, the cross-sectional area of the pipe is large enough that the minimum energy position of Xe does not lie at the center of the pipe at all values of z, and the shielding tensor is no longer axially symmetric. The minimum energy position of Xe is still along a more or less cylindrical locus of points coaxial with the pipe for a pipe with an approximately circular cross section, but the potential surface has hills and valleys on this inner cylinder, reflecting the atomistic nature of the pipe. As in the case of the medium-bore continuously smooth pipe (case C), when the Xe is close to the wall, there will be two components that are both more or less tangential to the wall surface (σ_t and $\sigma_{t'}$); the third component will be more or less perpendicular to the wall surface ($\sigma_\perp$). The orientation of the principal axis system (PAS) of the shielding tensor is the same as shown in case C, although in an atomistic pipe the tangential components may not necessarily line up exactly parallel and perpendicular to the axis of the pipe, especially at close distances. For the same reasons the relative values of the components are the same as in case C. We now consider a pipe with a noncircular cross section. As in case C, we consider limiting cases and find the same trends as the cross section becomes more elongated. (Refer back to the diagrams in case C, i.e., Figs. 3 and 4.) Thus, we find for a single Xe in a circular or elliptical medium-bore pipe

$$\sigma_\parallel<\sigma_t<\sigma_\perp<\sigma(\text{free Xe atom}).$$

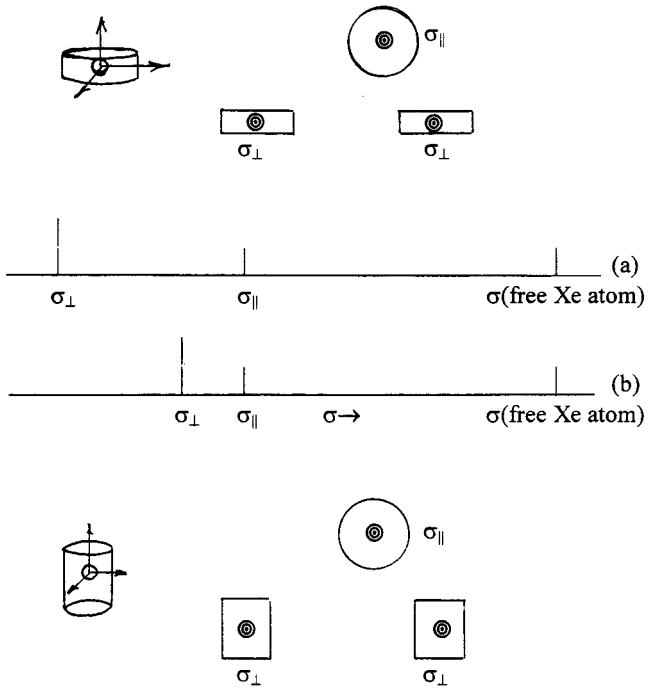

FIG. 5. Predicted shielding tensor components for a single Xe atom (a) in the limiting case of a very short capped pipe (a disk), and (b) in a capped pipe.

5. Capped pipes and disks

In the foregoing, we have considered smooth, open-ended pipes of indefinite length. Now, let us consider a Xe atom in capped pipes of finite length so that the predictions may be extended to Xe in cavities. One limiting case is a disk, a very short pipe that is capped at both ends. As before, we consider the shielding tensor components in terms of the Xe interactions with the walls. As shown in Fig. 5(a), both components are greatly deshielded relative to the Xe atom, $\sigma_{\parallel}$ to the same extent as for an open-ended pipe of indefinite length, and $\sigma_{\perp}$ even more strongly deshielded due to close interactions with both caps.

For a capped short pipe that accommodates no more than one Xe atom (length <8 Å, say), $\sigma_{\perp}$ will not be as deshielded as in the disk limit. The relative amounts of deshielding of $\sigma_{\parallel}$ and $\sigma_{\perp}$ relative to Xe atom will depend on the atomistic nature of the cap, and the length of the pipe. The closer the transverse circumference is to the cross-sectional ring, the more similar $\sigma_{\parallel}$ and $\sigma_{\perp}$ will be to each other. The predicted shielding tensor components for the capped short pipe are shown in Fig. 5(b), which also illustrates the relative magnitudes of the components compared to those in the limit of the disk.

B. At the high-loading limit

1. Case E (narrow-bore pipe)

When the pipe has a radius (r_{pipe}) such that the Xe minimum energy position is along the center of the pipe, and the pipe is fully occupied with Xe atoms, we may assume that the most important contributions to the shielding will be Xe–Xe interactions. Only two Xe neighbors (one above, one below the Xe atom in question) are required to account for nearly all the Xe–Xe contributions to the shielding; all other Xe atoms will be much farther away. The Xe–Xe interactions will give rise to large paramagnetic contributions to the $\sigma_{\perp}$ components but not to the $\sigma_{\parallel}$ component, leading to a large span for the shielding tensor, with both components deshielded compared to the free Xe atom, as predicted by the shielding tensor calculations for the linear Xe_3 trimer as a function of Xe–Xe distance (shown in Table VII). When the additional effects of the narrow-bore pipe are included, the expected result is as shown in Fig. 6.

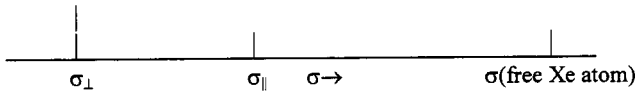

FIG. 6. The expected shielding components for Xe at full loading in a narrow-bore pipe. $\sigma_{\parallel}$ is the component along the axis of the pipe.

2. Case F (medium-bore pipe)

When the pipe has somewhat larger radius such that the Xe minimum energy position is away from the center of the pipe, and the pipe is highly occupied with Xe atoms, the most important contributions to the shielding will be Xe–Xe interactions. This will be similar to case E, except that the two perpendicular components will be quite similar, but no longer equivalent. The discrimination between the two perpendicular components will be greater at lower temperatures and will change markedly with loading, since Xe will not be lined up along the center of the pipe. Since the cross section of the pipe does not permit two Xe centers to be located in the same cross-sectional plane, then only two Xe neighbors (one above, one below the plane) are required to account for nearly all the Xe–Xe contributions to the shielding; all other Xe atoms will be much farther away. The angle α between the Xe–neighbor distance vectors at the minimum energy configuration, is determined by the atomistic nature of the pipe, as the string of Xe atoms in a fully loaded pipe comes into register with the atomic structure of the pipe itself.

First, let us consider the shielding of the unique Xe in a *free* symmetrical Xe_3 cluster (C_{2v}), with the angle α. The three components are: $\sigma_{\perp}$ (perpendicular to the molecular plane), $\sigma_{(C2)}$ (along the C_2 axis), $\sigma_{(\perp \text{ to } C2)}$ (in the molecular plane and perpendicular to the C_2 axis). In the limit of $\alpha = 180°$, $\sigma_{(C2)} = \sigma_{\perp}$ and $\sigma_{(\perp \text{ to } C2)}$ is $\sigma_{\parallel}$ (that is, along the axis of the pipe). The components change systematically as α decreases. For this discussion, we use as a basis the *ab initio* values shown in Table VII and VIII for Xe_3 systems at $\alpha = 180°$, 150°, 120°, and 60°. For $\alpha = 180°$, we find that

$$\sigma_{\perp} < \sigma_{\parallel},$$

with values $\sigma_{\perp} = -204.72$ and $\sigma_{\parallel} = +5.17$ ppm relative to the free Xe atom at 4.0 Å. For $\alpha = 60°$, we find that

$$\sigma_{\perp} < \sigma_{(\perp \text{ to } C2)} < \sigma_{(C2)}.$$

The values for $\alpha = 150°$ and 120° confirm the systematic changes one obtains by drawing the correlation diagram from the 180° to the 60° configuration, as shown in Fig. 7. There is a value of α (90°) at which the in-plane components

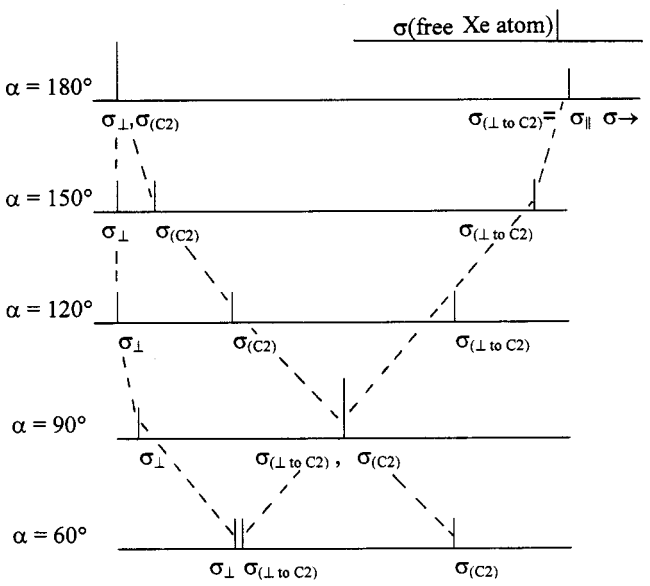

FIG. 7. The correlation diagram of the shielding components of Xe in a Xe_3 cluster, as the angle α changes from 180° to 60°.

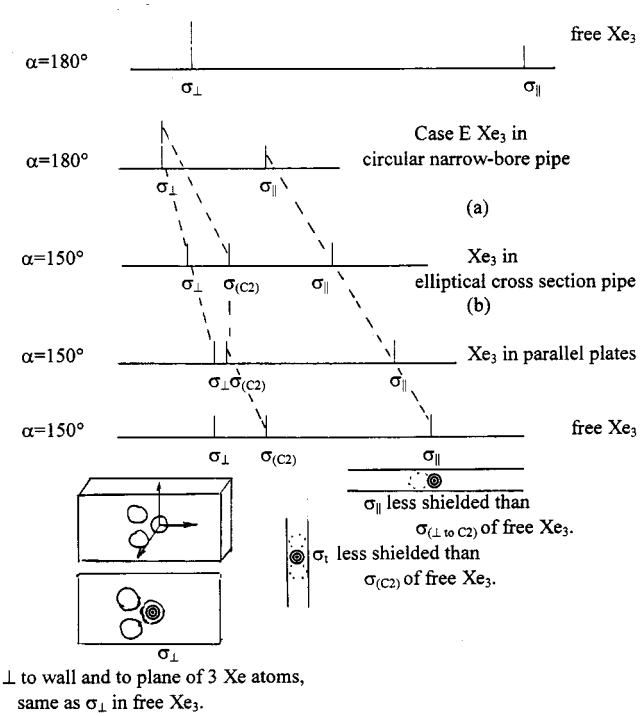

FIG. 8. The correlation diagram of the shielding components of Xe in a Xe_3 cluster in a pipe (a) as the Xe atoms achieve angles α from 180° (in a narrow-bore pipe), to smaller values in a pipe with an elliptical cross section, and (b) as the pipe changes from an elliptical cross section to the limiting case of parallel plates.

$\sigma_{(C2)}$ and $\sigma_{(\perp \text{ to } C2)}$ accidentally become identical. The *ab initio* values in Table VII and VIII confirm what we predicted from summing up the tensor contributions from Xe–Xe dimer in Table I.

Now, we consider the Xe_3 cluster in a medium-bore pipe. At full Xe loading, there will be a zigzag stack of Xe atoms as Xe goes into sites in register with the atomistic nature of the pipe. Since σ is a local property, however, we still only need to consider the environment of the central Xe in an Xe_3 cluster within the pipe, and $\sigma_{(C2)}$ becomes σ_t, and $\sigma_{(\perp \text{to } C2)}$ becomes $\sigma_\parallel$. Due to the interactions of the Xe with wall, $\sigma_{(\perp \text{to } C2)}$ becomes considerably less shielded compared to the free Xe_3, while $\sigma_\perp$ is less affected. The contributions of the interactions with the pipe and how this systematically changes with the cross-sectional shape of the pipe, can be understood by first consider the limiting case of Xe_3 between parallel plates. The definition of the tensor components is shown at the bottom of Fig. 8.

Using $\alpha = 150°$ as our example, the components of the bare Xe_3 will be affected by being placed between smooth parallel plates, as follows: $\sigma_{(\perp \text{to } C2)}$ and $\sigma_{(C2)}$ will be equally deshielded by the plates, while $\sigma_\perp$ will remain unchanged. Therefore, for Xe_3 at 150° between parallel plates, the order of $\sigma_\perp$ and (σ_t or $\sigma_{(C2)}$) is uncertain. Let us write the relative order as

$$\sigma_\perp \approx (\sigma_t \text{ or } \sigma_{(C2)}) < (\sigma_\parallel \text{ or } \sigma_{(\perp \text{ to } C2)}) < \sigma(\text{free Xe atom}).$$

At the other extreme, we similarly consider the effect of the narrow-bore pipe on the shielding of the center Xe in free Xe_3 at $\alpha = 180°$; $\sigma_\perp$ becomes deshielded, but $\sigma_\parallel$ is greatly deshielded, so the latter component moves much closer to $\sigma_\perp$. Next, we consider the systematic changes in the components while passing from Xe_3 in the slit between parallel plates, to Xe_3 in a circular narrow-bore pipe, as shown in Fig. 8. Thus, for Xe fully loaded into a pipe with an elliptical cross section, the most shielded component is likely to be $\sigma_\parallel$, i.e., $\sigma_{(\perp \text{to } C2)}$, so long as the angle α is fairly large, say around 150°. Depending on the nature of the pipe (as will be directly evidenced by the zero-loading Xe tensor in this pipe), the least shielded component will be either that perpendicular to the plane containing the Xe atom and its two nearest neighbors ($\sigma_\perp$) or the one in the plane containing these 3 Xe atoms and perpendicular to the axis of the channel (σ_t or $\sigma_{(C2)}$). All components are very much deshielded compared to the free Xe atom. For α around 150°

$$\sigma_\perp \approx \sigma_t < \sigma_\parallel < \sigma(\text{free Xe atom}).$$

C. Low loading

At low loading, only occasional Xe–Xe pairs contribute to the observed line shape. In the free Xe–Xe pair, two identical deshielded components are perpendicular to the Xe–Xe line (σ_{xx}); the third component is only slightly more shielded than the free Xe atom (σ_{zz}) and is along the Xe–Xe line. These tensor components in the free Xe_2 (*ab initio* values in Table I) will be resolved into $\sigma_\parallel$ and σ_t of Xe_2 in parallel plates according to the value of the tilt angle, θ: $\sigma_\parallel = \sigma_{B0}(\theta) = \sigma_{xx}\sin^2\theta + \sigma_{zz}\cos^2\theta$ and $\sigma_t = \sigma_{B0}(90° + \theta) = \sigma_{xx}\cos^2\theta + \sigma_{zz}\sin^2\theta$.

As before, we consider a Xe–Xe pair between parallel plates, at a tilt angle of 0°; the definition of the principal tensor components are shown at the bottom of Fig. 9. If we assume that the width of the pore is the same, σ_t will be deshielded relative to free Xe_2, and will be about the same for Xe_2 between parallel plates, Xe_2 in an elliptical bore, and

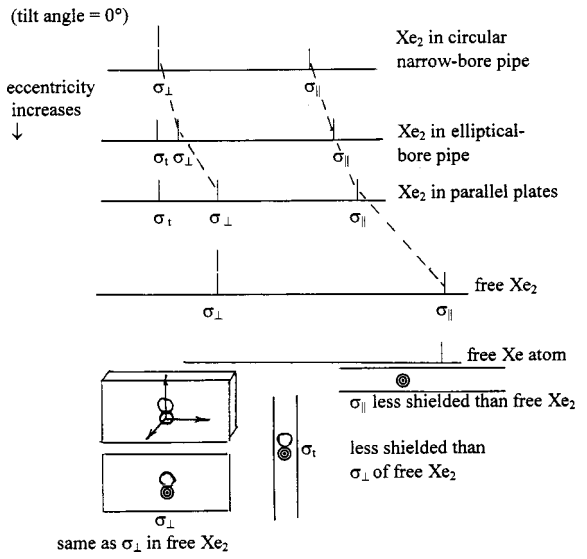

FIG. 9. The correlation diagram of the shielding components of Xe in a Xe_2 cluster in a pipe for tilt angle ≈0°, from circular narrow-bore pipe, to a pipe with an elliptical cross section, to the limiting case of parallel plates.

Xe_2 in a narrow-bore pipe (which is also for $\sigma_\perp$). $\sigma_\perp$ for Xe_2 between parallel plates will be the same as for the free Xe_2, whereas $\sigma_\perp$ for Xe_2 in an elliptical bore would be deshielded compared to free Xe_2, approaching $\sigma_\perp$ for Xe_2 in a circular narrow-bore pipe. For Xe_2 in an elliptical-bore pipe, $\sigma_\parallel$ will be less shielded than $\sigma_\parallel$ of Xe_2 in parallel plates, and approaching the $\sigma_\parallel$ of Xe_2 in a narrow-bore pipe. These trends are illustrated in Fig. 9.

We explicitly examine the effect of the tilt angle in Fig. 10. The tensor components for bare Xe_2 are taken from Table I, and modified as would be expected from the interactions with the walls. $\sigma_\perp$ is a unique component, that which is perpendicular to the wall *and* to the Xe–Xe line. The middle component will be $\sigma_\perp$ when the tilt angle is small. For a general tilt angle (but less than 90° since our definition of medium bore is that two Xe atoms cannot be in the same cross-sectional plane), $\sigma_\perp$ may be either greater or less than σ_t. The crossover point is 45° for the bare Xe_2 (e.g., at 4.0 Å

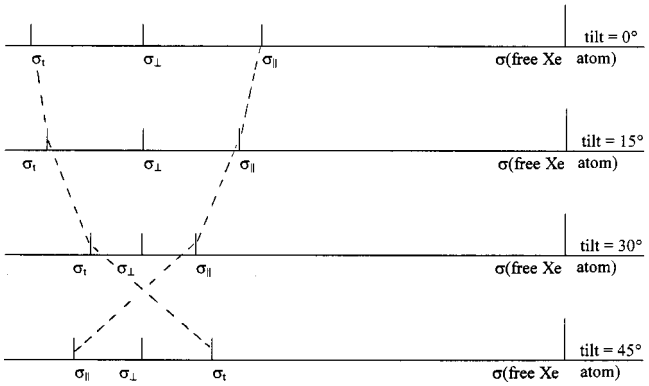

FIG. 10. The correlation diagram of the shielding components of Xe in a Xe_2 cluster in a pipe, as the angle (tilt angle) made by the Xe–Xe vector changes from 0° (in a narrow-bore pipe), to larger values in a pipe with an elliptical cross section. Approximate pipe contributions were added in to get this figure.

σ_t is −101 ppm at tilt angle of 0°, going to −75 ppm at 30° and −49 ppm at 45°, while $\sigma_\parallel$ is +2.5 ppm at tilt angle of 0°, going to −23 ppm at 30° and −49 ppm at 45°), but this is modified significantly by the interactions with the pipe. The tilt angle depends on the atomistic structure of the pipe which determines the locations of high probability density for Xe atoms. $\sigma_\perp$ remains about the same as the tilt angle changes.

Therefore, for Xe_2 in a pipe with an elliptical cross section

$$\sigma_t < \sigma_\perp < \sigma_\parallel < \sigma(\text{free Xe atom})$$

for a small tilt angle, close to 0°,

$$\sigma_\perp < \sigma_t < \sigma_\parallel < \sigma(\text{free Xe atom})$$

for a larger tilt angle.

At low loading, the Xe environment is *a thermal average* over the single Xe sites (same tensor as in the limit of zero loading) *and* the occasional Xe–Xe sites, as described above with the Xe_2 cluster in a pipe.

D. Temperature dependence

We consider here the temperature dependence of the shielding components of Xe in a pipe under zero- and full loading.

1. Case A (smooth narrow-bore pipe, zero loading)

The pipe has no corrugation, so there is no change in either potential energy or the shielding tensor with respect to position of Xe along the axis of the pipe. Since this is the case, the isotropic shielding and the line shape *should be temperature independent.*

2. Case B (narrow-bore pipe, zero loading)

As already discussed, the σ tensor will be axial at each z if symmetry at the cross-sectional plane is threefold or higher. U(Xe in pipe) will be a function of z; therefore, in this case the shape will be the same (axial anisotropy) but the span will change with z. Thus, as the thermal averaging over various positions along the center of the pipe is carried out, the width and the isotropic average will vary with temperature. The more shielded component $\sigma_\perp$ will remain nearly constant with temperature since diamagnetic changes are not very large, whereas both σ_{iso} and the less shielded component $\sigma_\parallel$ will change with temperature. With increasing temperature, $\sigma_\parallel$ will become more deshielded (assuming that at higher temperature, Xe will be able to spend more time in the more constricted part of the pipe, getting closer to the atoms in the cross-sectional plane). Thus, for a pipe with a bore small enough that the Xe position remains along the pipe center, increasing the temperature will lead to an increased deshielding in $\sigma_\parallel$, a decrease in σ_{iso}, and an increase in the span. These trends are illustrated in Fig. 11(a).

3. Case C (smooth medium-bore pipe, zero loading)

Since, as shown in Fig. 3, the three components change markedly as Xe moves closer to the wall surface, a marked temperature dependence of all components can be expected,

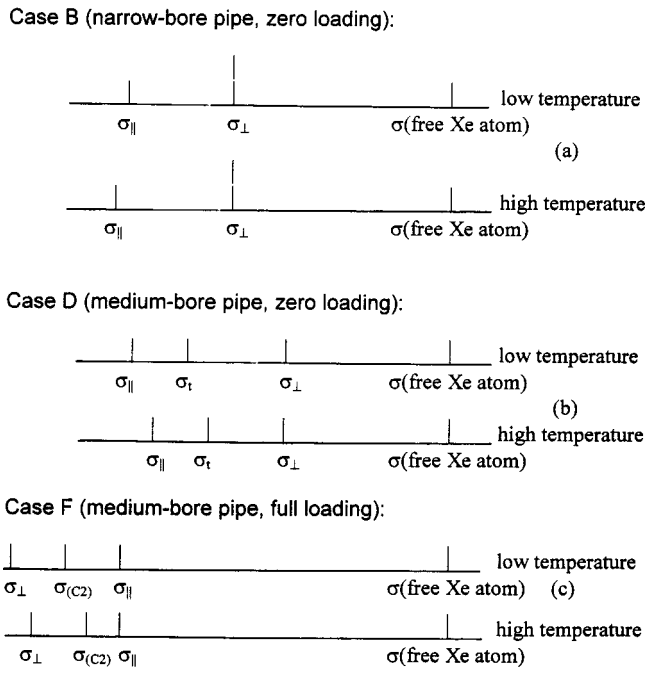

FIG. 11. Predicted temperature dependence of the Xe shielding components at zero and full loading.

with deshielding becoming less pronounced as Xe moves away from the wall surface and looks more like an isolated Xe atom. At lower temperatures, the Xe will spend more time in the favorable positions at $R=r_{\min}$, closer to the wall and farther from the center, so $\sigma_{\rm iso}$ will become less shielded, and the span will increase with decreasing temperature. These trends are illustrated in Fig. 11(b).

4. Case D (medium-bore pipe, zero loading)

The tangential components will change markedly as Xe moves closer to the curved surface; thus, a marked temperature dependence of these components can be expected. The deshielding becomes less pronounced as Xe moves away from the wall surface and looks more like an isolated Xe atom; thus, the span will decrease with increasing temperature. Of the three components, $\sigma_\perp$ will change less with temperature, deshielding with decreasing temperature, as Xe spends more time closer to the wall. At lower temperatures, the Xe will be closer to the wall, on the average, and $\sigma_{\rm iso}$ will become less shielded and the span will increase with decreasing temperature. At very high temperature, σ_t will become more like $\sigma_\perp$ and the line shape should approach the axial lineshape of case B. These trends are illustrated in Fig. 11(b).

5. Case E (narrow-bore pipe, full loading)

At the same Xe occupancy, no marked change with temperature is expected, if fully loaded. If less than fully loaded, the temperature dependence is less predictable, with more Xe clustering at low temperatures, but more deformations as Xe–Xe interactions intrude into the repulsive region of the potential energy surface at higher temperatures.

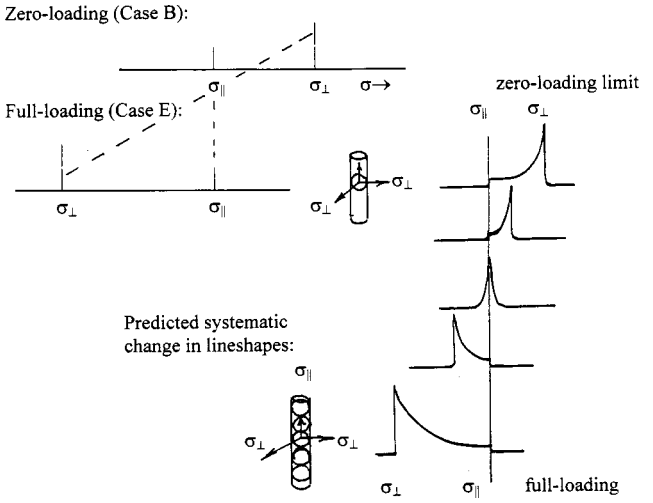

FIG. 12. Predicted systematic changes in Xe shielding components and line shapes, with increasing loading in a narrow-bore pipe.

6. Case F (medium-bore pipe, full loading)

We assume that the most significant temperature dependence is associated with lower temperature favoring Xe–Xe clustering, Xe–pipe interactions being less significant. $\sigma_\parallel$ is approximately the same, is nearly independent of temperature, since this component is primarily due to the Xe interactions with circle of atoms that make up the pipe. The least shielded component perpendicular to the plane containing the 3 Xe atoms ($\sigma_\perp$) should change the most with temperature since Xe–Xe contributions to shielding are involved. The middle component, $\sigma_{(C2)}$ or σ_t, approaches $\sigma_\perp$ as α approaches 180° (depending on the atomistic nature of the pipe) and changes with temperature accordingly, i.e., should change with temperature in the same direction as $\sigma_\perp$. These trends are illustrated in Fig. 11(e).

E. Variable loading

Here, we predict how the shielding components of Xe in a pipe change with increasing loading by considering each type of pipe.

1. Narrow-bore pipe

The minimum energy position for the Xe atom is at the center of the pipe. When the Xe occupancy is allowed to vary, as the situation moves from case B (near-zero loading) to case E (nearly full loading), the component that remains invariant with Xe loading is that one which arises primarily from interactions with the wall, $\sigma_\parallel$. This parallel component will remain unchanged, but it starts as the least shielded component in the zero-loading limit, and ends up the most shielded component in the high loading limit as the Xe–Xe interactions increasingly deshield the perpendicular components. The predicted systematic changes in line shape with increasing Xe loading in a narrow-bore pipe are shown in Fig. 12.

2. Medium-bore pipe, variable loading

When the Xe occupancy is allowed to vary, as the situation moves from case D (zero loading) to case F (full load-

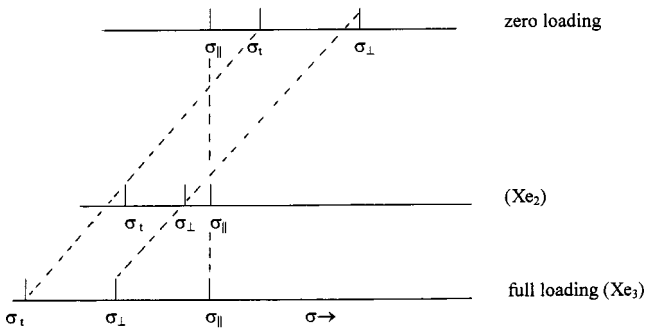

FIG. 13. Predicted systematic changes in Xe shielding components with increasing loading in a medium-bore pipe.

ing), the component that remains invariant with Xe loading is that which arises primarily from interactions with the wall, $\sigma_\parallel$. This parallel component will remain nearly unchanged, but starts out as the least shielded component in the zero-loading limit, and ends up the most shielded component in the high loading limit as the Xe–Xe interactions increasingly deshield the perpendicular components. Note that at low loading the Xe environment is an average over the single Xe sites (same tensor as in the limit of zero loading) and the occasional Xe–Xe sites, so the average line shape may have σ_t on either side of $\sigma_\parallel$. At lower temperatures, for modest loading, with at most Xe–Xe pairs in the pipe, the most deshielded component will be the one perpendicular to the wall and to the Xe–Xe line of centers ($\sigma_\perp$). The least shielded component is perpendicular to the plane containing the 3 Xe atoms ($\sigma_\perp$); since Xe–Xe contributions to shielding are involved this component should change the most with loading. The middle component is in the plane containing the 3 Xe atoms and is perpendicular to the axis of the channel (σ_t). It changes with loading in the same direction as $\sigma_\perp$. Therefore, for a medium-bore pipe the effect of changing loading (at the same temperature) is as shown in Fig. 13.

IV. COMPARISONS WITH EXPERIMENT

A. Predictions versus observations

In order to compare with experiment, we have to keep in mind the nature of the averaging that takes place. We have used as models nanochannels of indefinite length. When the crystallites which provide the channels are of sufficient size that the ratio of channel length to diameter is very large, this limit is essentially reached. The contributions to the line shape come from Xe atoms that explore only one channel whose axis is at a particular fixed orientation in the magnetic field. When the crystallites are very finely powdered, the intercrystallite diffusion rate is high; a Xe atom that contributes to the line shape will have sampled many channels at various orientations and reports a highly averaged chemical shift, in which case the powder pattern becomes collapsed, and the anisotropic line shape approaches the isotropically averaged shape observed in liquids. We considered only cases where the Xe is unable to execute an isotropic average by restricting the pipe cross-sectional areas to those which do not permit the Xe atoms to pass each other in the channel

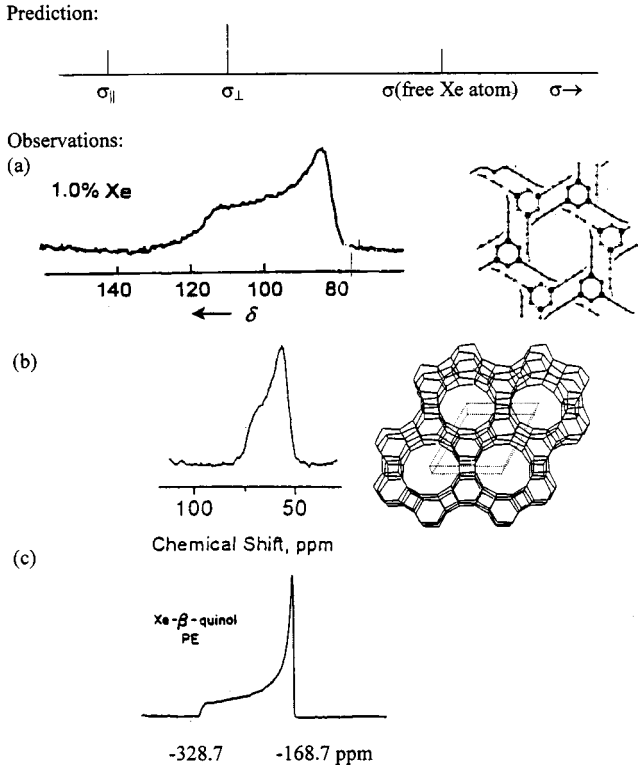

FIG. 14. Examples of Xe in a narrow-bore pipe: (a) Xe at very low concentration in tris(*o*-phenylenedioxy)cyclotriphosphazene, TPP, spectrum reported by Sozzani *et al.* (Ref. 35). (b) Xe at a very low concentration in the highly siliceous zeolite SSZ-24, spectrum reported by Moudrakovski *et al.* (Ref. 37). (c) One example of a not quite long enough channel is β-quinol clathrate, which has a 4.2 Å free diameter, and free length 6.7 Å, spectrum reported by Ripmeester. (Ref. 30).

and by considering channels that are indefinitely long. Thus, the anisotropic line shape persists when the dynamic averaging experienced by a particular Xe atom occurs entirely within one channel and effectively only along the direction of the pipe axis. With few exceptions, the bulk of anisotropic line shapes for Xe in various channel or cavity types have been reported by Ripmeester and co-workers.

Our prediction of the tensor components for a single Xe in a narrow-bore pipe (case B) can be compared with experiments at the zero-loading limit. We show two examples of Xe in one-dimensional channel systems in Fig. 14. Xe at very low concentration in tris(*o*-phenylenedioxy)cyclotriphosphazene or TPP has been observed by Sozzani, Pines, and co-workers at the level of 1 mole % Xe in a $He–N_2$ stream, using hyperpolarized Xe in a continuous flow system.[35] The channel structure with a 4.5 Å diameter is formed by the hexagonal crystal packing of TPP. One example of Xe in a not quite long enough channel is Xe in β-quinol clathrate, which has a cavity 4.2 Å free diameter, and free length 6.7 Å, but nevertheless exhibits the same Xe shielding tensor anisotropy[30] as we predict for a Xe atom in an indefinitely long narrow-bore pipe. The line shape prediction is the same for a Xe in a medium-bore symmetrical pipe under conditions in which the Xe is spending most of its time along the axis of the pipe. Under continuous flow conditions, hyperpolarized Xe at the zero-loading limit in SSZ-24 has been observed.[36,37] The SSZ-24 zeolite has one-dimensional

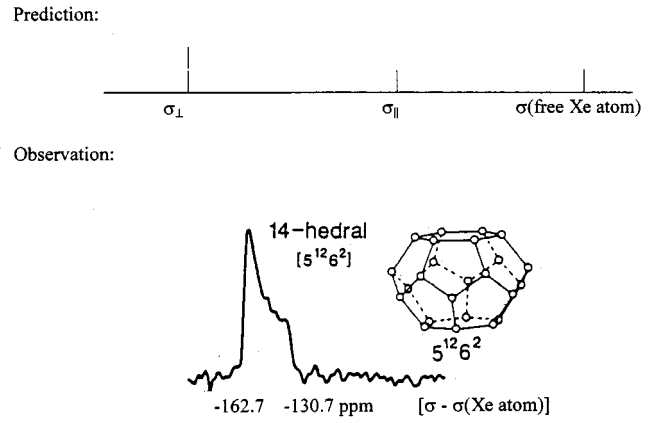

FIG. 15. An example of Xe in a disk. A single Xe atom observed in the larger cage ($5^{12}6^2$) of structure I hydrate at 77 K, spectrum reported by Ripmeester *et al.* (Ref. 31).

channels that are formed by a symmetrical 12-oxygen ring of 7.3 Å diameter. These examples are shown in Fig. 14.

Our prediction for the extreme case of a single Xe in a disk is an axially symmetric tensor with the $\sigma_\perp$ as the least shielded component. A single Xe atom in the larger cage ($5^{12}6^2$) of structure I hydrate at 77 K exhibits just the predicted line shape, greatly deshielded relative to the free Xe atom. This is a cage that is approximately a very short, squat cylinder, the opposite of a long pipe. Xe is in close interactions with the top and bottom of the cage that is effectively a disk.[31] This example is shown in Fig. 15 and provides the experimental signature for the formation of clathrate hydrates in the extensive work on these systems by Ripmeester *et al.* Other examples of Xe trapped inside a disk are Xe in the 5^{12} cage of clathrate hydrate type II, in which the caps are made up of parallel $(OH)_5$ rings, and Xe in the silica analog of this structure, with very nearly the same geometry, also given in this work.[31]

The prediction for Xe in full loading in a narrow-bore pipe is coincidentally the same line shape as for a single Xe atom in a disk. Shown in Fig. 16 are prediction and observations. The Xe doubly occupied cages in DD3R zeosil at room temperature and (top) and at ~200 K (bottom), another example from Ripmeester *et al.*,[33] show the predicted line shape and also the predicted temperature dependence [larger span at lower temperature, shown in Fig. 11(a)]. Using a 100% Xe continuous stream of hyperpolarized xenon leads to a very a high occupancy of Xe in tris(*o*-phenylenedioxy)cyclotriphosphazene, so the observed line shape[35] corresponds to that in the limit of full loading in a narrow-bore pipe. Indeed, the entire sequence of spectra obtained for Xe in the nanochannels of TPP at various mole fractions of Xe in the gas stream (reproduced in Fig. 17) corresponds to the predicted sequence with increasing Xe loading in a narrow-bore pipe, illustrated in our prediction in Fig. 12. As the mole fraction of Xe in the gas stream is increased while keeping the flow rate the same, the average Xe occupancy of the nanochannels increases. Spectra taken at the same flow rate and the same Xe mole fraction in the gas stream, but with decreasing temperature, would lead to

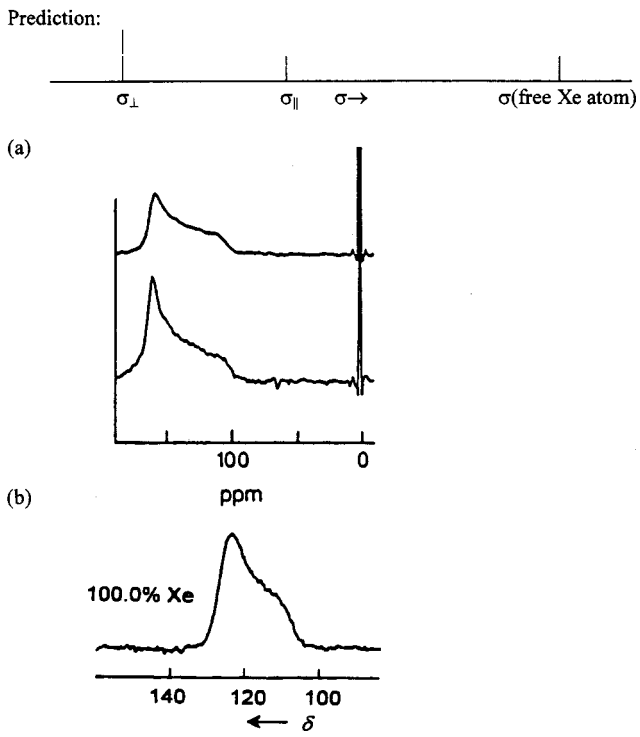

FIG. 16. Examples of Xe at high loading in a narrow-bore pipe. (a) Xe doubly occupied cages in DD3R zeosil at room temperature (top) and at ca. 200 K (bottom), spectrum from Ripmeester *et al.* (Ref. 33). (b) 100% Xe in a continuous flow hyperpolarized system observed in tris(*o*-phenylenedioxy)cyclotriphosphazene, TPP, from Sozzani *et al.* (Ref. 35).

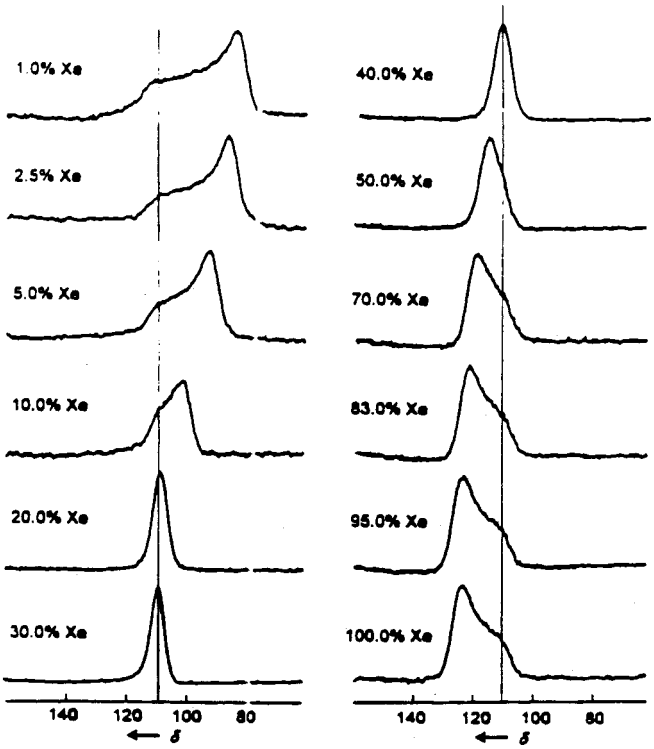

FIG. 17. Xe NMR spectra observed as a function of concentration in tris(*o*-phenylenedioxy)cyclotriphosphazene or TPP, reported by Sozzani *et al.* (Ref. 35) compare very favorably with our predictions in Fig. 12.

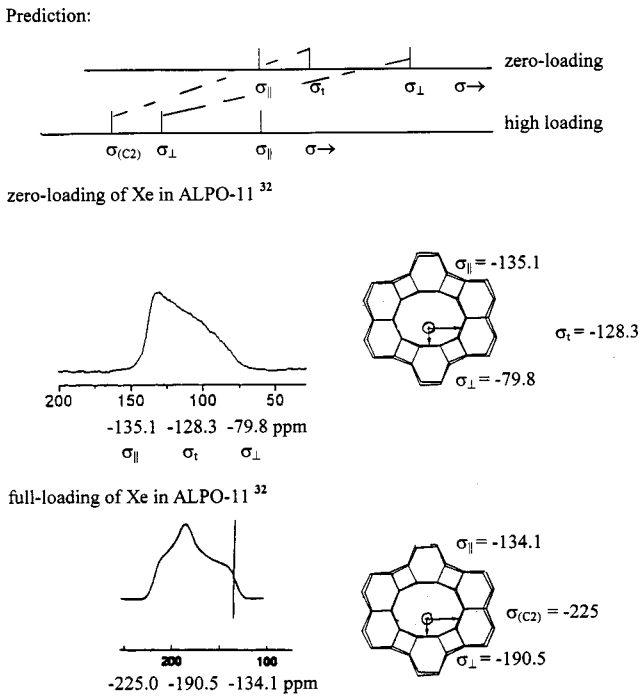

FIG. 18. Xe spectra at the extreme loading limits: *Zero-loading* (case D): ($\sigma_\perp$ perpendicular to wider wall, σ_t tangential to the wide wall, and perpendicular to channel axis, $\sigma_\parallel$ parallel to channel axis). *High-loading*: nonlinear Xe string along the wall ($\sigma_\perp$ perpendicular to the plane containing the 3 Xe atoms; $\sigma_{(C2)}$ in the plane containing the 3 Xe atoms and perpendicular to the axis of the channel, $\sigma_\parallel$ parallel to channel axis).

increasing Xe occupancy in the nanochannels, thus, the sequence of spectra would again be expected to follow the predicted line shape changes with loading in Fig. 12, and indeed they do.[35]

The temperature dependence predicted in Fig. 11(c) for medium-bore pipes at full Xe loading has been observed in silicalite.[25] Silicalite has full loading of 16 Xe atoms per unit cell, but it is more complex in that it has sinusoidal channels as well as the straight elliptical channels. Nevertheless, the cross section is such that Xe atoms cannot pass each other in the channels as they diffuse. The least shielded component (perpendicular to the plane containing the Xe atom and its two nearest neighbors) $\sigma_\perp$, changed the most, whereas $\sigma_\parallel$ (along the direction of the channel axis) hardly changed at all. We assign the components $\sigma_\perp$, σ_t, $\sigma_\parallel$, respectively, to our observed values[25]

-199.3 -189.4 -161.9 ppm at 240 K,
-193.4 -185.6 -163.5 ppm at 270 K,
-187.9 -179.4 -163.5 ppm at 300 K.

The trends with decreasing temperature are just as predicted in Fig. 11(c).

For Xe in medium-bore channels with elliptical cross sections, our predictions in Fig. 13 match the spectra of Xe observed as a function of loading in ALPO-11.[32] In Fig. 18 we show only the zero-loading and the full-loading limit predictions, and we assign the average tensor components observed to the appropriate principal axes directions. The one assigned to $\sigma_\parallel$ hardly changed with increasing loading, since the contributions to it come entirely from the ring of atoms that forms the elliptical bore. On the other hand, the $\sigma_\perp$, which is along a perpendicular to the wall, is the least deshielded since the contributions to it come only from the two distant atoms of the ellipse that are coplanar with the single Xe atom. At full loading, however, coplanar with the Xe atom are two other Xe atoms, leading to a very deshielded $\sigma_\perp$. The tangential component σ_t for the single Xe atom is somewhat more deshielded than the perpendicular component, since the contributions to it come from the two somewhat closer atoms of the ellipse that are coplanar with the single Xe atom. At full loading, coplanar with the Xe atom are two other Xe atoms, leading to a very deshielded σ_t.

V. DISCUSSIONS

What is the nature of the information that we can obtain from the Xe shielding tensor of a Xe atom in a nanopipe? Since the parallel component $\sigma_\parallel$ of the Xe shielding tensor is the one that is most sensitive to the rings of atoms that form the cross section of the pipe, then the value of $\sigma_\parallel$ at the zero-loading limit contains information about the pipe diameter and its structure. If the pipe is capped at the ends, then the value of $\sigma_\perp$ at the zero-loading limit gives an accounting of the atomistic nature of the cap and also how long the pipe is. On the other hand, the value of $\sigma_\perp$ at the intermediate-or full-loading limit is primarily a measure of the range of Xe–Xe distances that are averaged over, in effect it is a measure of the Xe–Xe distance distribution function along the axis of the pipe. A pipe loaded to saturation will have a very deshielded value of $\sigma_\perp$. The extreme case, at very close Xe–Xe distances, would be comparable to σ in solid Xe near 0 K.

Let us consider some examples. The value of $\sigma_\parallel$ at the zero-loading limit (and in a narrow-bore pipe, for all loading levels) contains information about the pipe diameter and its structure. (All numerical values of shielding given in the discussion below are quoted relative to the shielding of the free Xe atom and are taken at room temperature.) The extreme values found are $\sigma_\parallel = -343$ ppm in the small cage of the β phenol clathrate and -328.7 in the β quinol cage.[30] Both have a ''free diameter'' of about 4.2 Å. In the slightly larger cage (4.3 Å free diameter) of the β phenol clathrate, $\sigma_\parallel$ is -320 ppm. These very deshielded values are very unusual and indicate very significant interactions indeed between Xe and the pipe. These are among the most deshielded components observed for Xe atom in any environment, comparable to that in solid Xe at 21 K.[46] In the 12-hedral cage of clathrate hydrate type II, in which the free diameter is 5.1 Å, Xe has $\sigma_\parallel = -213$ ppm, and in the silica analog of this, clathrasil dodecasil-3C, $\sigma_\parallel = -205$ ppm.[31] In ALPO-11 which has a rather larger cross-sectional area (3.9×6.3 Å), it is -135.1 ppm.[32] Here, the Xe interacts with a ring of 10 bridging O atoms that are attached to tetrahedral P and Al. In silicalite, which has straight channels that are 5.3×5.6 Å, and sinusoidal channels that are 5.1×5.5 Å, $\sigma_\parallel$ is -163.5 ppm.[25] Here, the Xe interacts with 10 bridging O atoms that are all attached to Si. A smaller value, $\sigma_\parallel = $ ca. -75 ppm, is found in zeolite SSZ-24, where the channels have a free diameter of 7.3 Å and Xe interacts with 12 bridging O atoms attached to tetrahedral Si.[36,37] In a fully hydrated

α-cyclodextrin macrocycle, consisting of six anhydroglucose units bonded head to tail, Xe has $\sigma_{\parallel}=-177$ ppm.[31] In the 14-hedral cage of structure I hydrate clathrate, in which a ring of 12 staggered O atoms form a very short pipe with a free diameter of 6.6 Å, Xe has $\sigma_{\parallel}=-130.7$ ppm.[29] In contrast, in the molecular crystal TPP, Xe interacts with the faces of the staggered aromatic rings that form the hexagonal pipe that has a free diameter of about 4.5 Å, and here Xe has $\sigma_{\parallel}$ ca. -110 ppm, not nearly as deshielded as in other pipes with the same free diameter.

In capped pipes, the value of $\sigma_{\perp}$ at the zero-loading limit gives an accounting of the atomistic nature of the caps and also how long the pipe is. The two flat $(OH)_5$ rings that trap the Xe atom in the disk-shaped 12-hedral cage of the structure II hydrate clathrate are 6.1 Å apart, and gives a very deshielded Xe shielding component of $\sigma_{\perp}=-231$ ppm, and $\sigma_{\perp}=-250$ ppm in the silica analog (clathrasil dodecasil-3C) of very similar dimensions.[31] Xe trapped between the two flat $(OH)_6$ rings in the 14-hedral cage of the structure I clathrate hydrate, which are 6.02 Å apart, exhibits a shielding component of -162.7 ppm.[29] In the β-phenol and the β-quinol clathrates, the $(OH)_6$ caps of the cages give rise to similar shielding components of $\sigma_{\perp}=-172$ and -168.7 ppm, respectively. These are short pipes, about 6.7 Å long, occupied by only one Xe atom.[30]

The value of $\sigma_{\perp}$ at the intermediate-or full-loading limit is primarily a measure of the range of Xe–Xe distances that are averaged over; in effect, it is a measure of the Xe–Xe distance distribution function along the axis of the pipe. Values range from -170 to -261 ppm relative to the free Xe atom. (There is the TPP case, where $\sigma_{\perp}=-125$ ppm for a pure Xe gas stream, but it is uncertain whether maximum Xe loading is achieved under these flow conditions.[35]) For example, in the β-phenol clathrate cage that has a length of $\sim$15 Å and a free diameter of 4.3 Å, at full loading of 3 Xe atoms, the end Xe atoms have $\sigma_{\perp}=-215$ ppm, whereas the central Xe atom has $\sigma_{\perp}=-261$ ppm. These may be compared to full loading (8 Xe atoms) in the more symmetrical α cages of NaA (cagelength=12.28 Å), where $\sigma=-272.3$ ppm.[47] Full loading in elliptical medium-bore pipes lead to $\sigma_{\perp}$ and $\sigma_{\perp'}=-187.9$ and -179.4 ppm in silicalite,[25] -225 and -190.5 in ALPO-11, where the Xe atoms are staggered within the elliptical pipes.[32] These values may be compared to Xe in solid Xe, in which $\sigma=-275$ to -310 ppm, becoming more deshielded at higher densities.[46]

In passing, we reiterate that in predicting the line shape we have made the assumption that Xe–Xe interactions dominate over Xe–ring interactions. This appears not to hold in the β-quinol and the β-phenol clathrates, where the interactions of a single Xe atom with the pipe are very significant, as evidenced by the extremely deshielded values of $\sigma_{\parallel}$. In the β-quinol and the β-phenol clathrates, the Xe shielding anisotropy does not change sign, $\sigma_{\parallel}<\sigma_{\perp}$, even for the fully loaded pipe, in contrast with other cases described here.

Are the neighbor contributions to the shielding components additive? We can compare in Table VI the *ab initio* shielding components of one Xe atom surrounded by 6 or 8 Ne atoms at a distance of 4.0 Å with one another: $\sigma_{\parallel}-\sigma(\text{Xeatom})=-16.00$ ppm is found for an 8-Ne ring, whereas -17.21 ppm would have been expected from a strictly additive situation, based on -12.91 ppm for a 6-Ne ring. Similarly, the $\sigma_{\perp}-\sigma(\text{Xeatom})=-7.68$ ppm is found for the 8-atom ring, whereas -7.59 ppm would have been expected from the 6-atom ring value. In particular, it is interesting to observe the additivity of the Xe–Xe contributions to $\sigma_{\perp}$. For example, for a single Xe atom in the β-phenol clathrate cage of $\sim$15 Å length, $\sigma_{\perp}$ should be about the same as in the cage of $\sim$6.7 Å length, -170 ppm, since the caps are about the same when the 15 Å cage is occupied by the maximum of 3 Xe atoms. Each neighboring Xe inside the cage with it contributes -45 ppm to $\sigma_{\perp}$, i.e., from -170 ppm to the observed -215 ppm, then another -45 ppm increment for another Xe neighbor takes $\sigma_{\perp}$ to the observed -261 ppm.[30] Similarly, in ALPO-11, to $\sigma_{\perp}=-128.3$ ppm for a single Xe in the channel, one Xe neighbor contributing -48.3 ppm leads to -176.6 ppm and then another -48.3 ppm increment for a second Xe neighbor leads to the observed -225 ppm.[32] The σ_t or $\sigma_{(C2)}$ likewise increments by -55.3 ppm, starting from -79.8 ppm to -135.1 ppm to -190.5 ppm. This validates within experimental error, the tensor $(\sigma_{\parallel},\sigma_{\perp},\sigma_t)=(-135.1,-177.3,-134.6$ ppm) proposed for Xe_2 in an ALPO-11 channel, arrived at by Ripmeester *et al.*,[32] by using a binomial distribution for the Xe atoms among the adsorption sites in the analysis of the variation of the line shape with Xe loading. The Xe_2 in the pipe accidentally has an axially symmetric shielding tensor, and indeed, at exactly half-loading a line shape consistent with an axially symmetric σ is observed. Ripmeester *et al.* stated that they could not establish from their experiments which sets of tensor components correspond to which channel axis.[32] With the analysis described here, the directions of the tensor principal axes can be assigned as follows: For a single Xe atom in the channel: $(\sigma_{\parallel},\sigma_t,\sigma_{\perp})=(-135.1,-128.3,-79.8$ ppm) in which $\sigma_{\parallel}$ is along the channel axis, σ_t is parallel to the long axis of the ellipsoid cross section, and $\sigma_{\perp}$ is parallel to the short axis. For Xe_2, the latter accidentally becomes the same as the component along the axis of the channel. For the central Xe of Xe_3 in the channel, the axis assignments are $(\sigma_{\parallel},\sigma_t,\sigma_{\perp})=(-135.1,-225,-190.5$ ppm). The somewhat larger deshielding increment per Xe neighbor parallel to the short axis of the ellipsoid cross section, -55.3 ppm, compared to the component parallel to the long axis, is a consequence of the value of the angle α described in the text, as determined by the atomistic nature of the channel wall which dictates the locations of the lowest energy positions for Xe in the channel. The latter has been well described by Ripmeester *et al.*,[32] who explicitly recognized for the first time that the experimental line shape is the result of dynamic averaging of the shielding tensors.

The additivity of the Xe–Xe contributions noted here has a theoretical basis in the *ab initio* calculations for the ^{129}Xe shielding in the free Xe_3 system in linear and equilateral triangle arrangements with variable internuclear separations. For all distances greater than r_0 (the distance at which the potential function is zero for Xe–Xe dimer), reasonably good additivity in σ_{iso} was observed.[2] In Table VIII, the cal-

culated tensor components are used to illustrate the incremental contributions of each Xe–Xe interaction to the shielding. To put the distances in context, it should be noted that the distance at which the potential energy is zero for Xe–Xe pair is 4.0 Å. Additive components from each neighbor appear to be a good approximation for the configuration with $\alpha = 180°$, at Xe–Xe distances of 4.4 Å and longer, even at the close Xe–Xe distance of 4.0 Å. On the other hand, for the configuration with $\alpha = 60°$, deviations from the additivity assumption are somewhat larger at Xe–Xe distances of 4.4 Å and longer, becoming very significant at Xe–Xe distances of 4.0 Å, especially for the component perpendicular to the plane containing the atoms (42.7 ppm). This is easily understood. In the triangular arrangement, unlike the linear arrangement, the neighboring atoms do interact significantly with one another, leading to large changes in electron distribution, compared to that in isolated Xe_2 from which the additive components are derived.

VI. CONCLUSIONS

The spectral line shapes of Xe in limiting cases of nanochannels have been considered. The results of *ab initio* calculations enlighten the consideration of various limiting cases, and correlation diagrams for the tensor components of the limiting cases permit the prediction of more general cases such as the shielding tensor of Xe in medium-bore channels with elliptical cross sections. The progression of line shapes from zero loading through intermediate and full loading and also the temperature dependence at fixed loading are predicted. Comparisons with experiment are possible in those cases where the exchange of Xe between the gas phase and the nanopores is sufficiently slow so that the average Xe environment within the nanopore is reflected by the shielding observed. The predictions are in agreement with available experimental data. It is proposed that the shielding tensors of Xe atoms in nanochannels are systematically influenced by the size, shape, and atomistic structure of the channel. With the general predictions made here, the experimental line shapes obtained for Xe in novel nanostructural environments may be understood.

ACKNOWLEDGMENTS

This research is supported by the National Science Foundation (Grant No. CHE99-79259), which is hereby gratefully acknowledged. This work was inspired by Professor Alexander Pines and Professor Piero Sozzani and their colleagues Roberto Simonutti, Angiolina Comotti, and Thomas Meersman during the XEMAT 2000 Conference on Optical Polarization and Xenon NMR of Materials.

[1] W. T. Raynes, A. D. Buckingham, and H. J. Bernstein, J. Chem. Phys. **36**, 3481 (1962).
[2] C. J. Jameson and A. C. de Dios, J. Chem. Phys. **97**, 417 (1992).
[3] H. F. A. Rummens and F. Mourits, Can. J. Chem. **55**, 3021 (1977).
[4] A. D. Buckingham, Can. J. Chem. **38**, 300 (1960).
[5] F. H. A. Rummens, Chem. Phys. Lett. **31**, 596 (1975).
[6] T. R. Stengle, N. V. Reo, and K. L. Williamson, J. Phys. Chem. **85**, 3772 (1981).
[7] J. Fraissard and T. Ito, Zeolites **8**, 350 (1988).
[8] Q. J. Chen and J. Fraissard, J. Phys. Chem. **96**, 1809 (1992).
[9] T. T. P. Cheung, C. M. Fu, and S. Wharry, J. Phys. Chem. **92**, 5170 (1988).
[10] D. Raftery, L. Reven, H. Long, A. Pines, P. Tang, and J. A. Reimer, J. Phys. Chem. **97**, 1649 (1993).
[11] S. B. Liu, B. M. Fung, T. C. Yang, E. C. Hong, C. T. Chang, P. C. Shih, F. H. Tong, and T. L. Chen, J. Phys. Chem. **98**, 4393 (1994).
[12] J. L. Bonardet, J. Fraissard, A. Gedeon, and M. A. Springuel-Huet, Catal. Rev. Sci. Eng. **41**, 115 (1999).
[13] D. M. Bishop and S. M. Cybulski, Chem. Phys. Lett. **211**, 255 (1993).
[14] D. M. Bishop and S. M. Cybulski, J. Magn. Reson., Ser. A **107**, 99 (1994).
[15] M. Bühl, M. Kaupp, O. L. Malkina, and V. G. Malkin, J. Comput. Chem. **20**, 91 (1999).
[16] P. O. Åstrand, K. V. Mikkelsen, K. Ruud, and T. Helgaker, J. Phys. Chem. **100**, 19771 (1996).
[17] P. O. Åstrand, K. V. Mikkelsen, P. Jørgensen, K. Ruud, and T. Helgaker, J. Chem. Phys. **108**, 2528 (1998).
[18] K. V. Mikkelsen, K. Ruud, and T. Helgaker, Chem. Phys. Lett. **253**, 443 (1996).
[19] K. V. Mikkelsen, P. Jorgensen, K. Ruud, and T. Helgaker, J. Chem. Phys. **106**, 1170 (1997).
[20] C. J. Jameson, A. K. Jameson, B. I. Baello, and H. M. Lim, J. Chem. Phys. **100**, 5965 (1994).
[21] C. J. Jameson, A. K. Jameson, H. M. Lim, and B. I. Baello, J. Chem. Phys. **100**, 5977 (1994).
[22] C. J. Jameson, A. K. Jameson, R. E. Gerald II, and H.-M. Lim, J. Chem. Phys. **103**, 8811 (1995).
[23] C. J. Jameson, A. K. Jameson, and H. M. Lim, J. Chem. Phys. **104**, 1709 (1996).
[24] C. J. Jameson and H. M. Lim, J. Chem. Phys. **107**, 4373 (1997).
[25] C. J. Jameson, A. K. Jameson, R. E. Gerald II, and H. M. Lim, J. Phys. Chem. B **101**, 8418 (1997).
[26] C. J. Jameson, H. M. Lim, and A. K. Jameson, Solid State Nucl. Magn. Reson. **9**, 277 (1997).
[27] C. J. Jameson, A. K. Jameson, A. C. de Dios, R. E. Gerald II, H. M. Lim, and P. Kostikin, in *Modeling NMR Chemical Shifts: Gaining Insights into Structure and Environment*, ACS Symposium Series 732, edited by J. C. Facelli and A. C. de Dios (Oxford University Press, Oxford, 1999), pp. 335–348.
[28] C. J. Jameson, A. K. Jameson, P. Kostikin, and B. I. Baello, J. Chem. Phys. **112**, 323 (2000).
[29] J. A. Ripmeester and D. W. Davidson, J. Mol. Struct. **75**, 67 (1981).
[30] J. A. Ripmeester, J. Am. Chem. Soc. **104**, 289 (1982).
[31] J. A. Ripmeester, C. I. Ratcliffe, and J. S. Tse, J. Chem. Soc., Faraday Trans. 1 **84**, 3731 (1988).
[32] J. A. Ripmeester and C. I. Ratcliffe, J. Phys. Chem. **99**, 619 (1995).
[33] J. A. Ripmeester and C. I. Ratcliffe, Mater. Res. Soc. Symp. Proc. **233**, 281 (1991).
[34] M. A. Springuel-Huet and J. Fraissard, Chem. Phys. Lett. **154**, 299 (1989).
[35] P. Sozzani, A. Comotti, R. Simonutti, T. Meersmann, J. W. Logan, and A. Pines, Angew. Chem. Int. Ed. Engl. **39**, 2695 (2000).
[36] I. Moudrakovski, A. Nosso, S. Lang, C. Ratcliffe, and J. A. Ripmeester, NMR Symposium, 42nd Rocky Mountain Conference, Broomfield, CO, 30 July–3 August 2000.
[37] I. Moudrakovski, A. Nossov, S. Lang, S. R. Breeze, C. Ratcliffe, B. Simard, G. Santyr, and J. A. Ripmeester, Chem. Mater. **12**, 1181 (2000).
[38] C. J. Jameson and A. C. de Dios, in *Nuclear Magnetic Shielding and Molecular Structure*, edited by J. A. Tossell (Kluwer Academic, Dordrecht, 1993), pp. 95–116.
[39] A. C. de Dios and C. J. Jameson, J. Chem. Phys. **107**, 4253 (1997).
[40] M. J. Frisch, G. W. Trucks, and H. B. Schlegel *et al.*, GAUSSIAN 98, Revision A.7, Gaussian, Inc., Pittsburgh, PA, 1998.
[41] H. Partridge and K. Faegri, NASA Technical Memo 103918 (1992).
[42] D. A. Bishop and S. M. Cybulski, Chem. Phys. Lett. **211**, 255 (1993).
[43] S. Huzinaga, *Gaussian Basis Sets for Molecular Calculations* (Elsevier, Amsterdam, 1984).
[44] A. C. de Dios, D. Sears, and C. J. Jameson (unpublished).
[45] C. J. Jameson and A. C. de Dios, J. Chem. Phys. **98**, 2208 (1993).
[46] D. Brinkmann and H. Y. Carr, Phys. Rev. **150**, 174 (1966).
[47] C. J. Jameson, A. K. Jameson, R. E. Gerald II, and A. C. de Dios, J. Chem. Phys. **96**, 1676 (1992).